Benchmarking the Linear and non-Linear Elastic Properties of Group-III Nitrides

Nikita Winter

A thesis presented for the degree of
"Bachelor of Science"

Humboldt-Universität zu Berlin
Faculty of Mathematics and Natural Sciences
Department of Physics

Examiners:

1) PD Pasquale Pavone

2) Prof. Claudia Draxl

Thesis submitted on March 18, 2024

Abstract

We present *ab-initio* calculations of the elastic properties of the group-III nitrides. The calculations are performed using density-functional theory as implemented in the **exciting** code. The software tool **ElaStic** is used as pre and post-processing for the elastic properties. Both second and third-order elastic constants are calculated for the zincblende phase of these materials. We provide a benchmark for analysing the elastic properties of these materials in terms of the convergence with respect to a selected set of numerical parameters. In order to enable the possibility of using automatized workflows for the determination of elastic constants without explicit human intervention, we introduced the δ-parameter method. This method is used to automatize the interpretation of the polynomial fits which are used for calculating finite-difference derivatives of the elastic energy.

Contents

Chapter 1

Introduction

The group-III nitrides (BN, AlN, GaN, and InN) all have different physical properties. For example, while boron nitride (BN) is well known to be very hard and brittle, indium nitride (InN) is much less brittle and softer. BN is the second hardest material after diamond and is used often on metallic cutting tools for cutting hard steels [1]. AlN has a high thermal conductivity, a low conductive of thermal expansion, good electrical resistance and is a semiconductor. That makes AlN a good solid for electrical applications and thermal management. Because it is cheap and safe, it is the leading material in the production of hybrid microcircuits [2]. GaN has a high power density, a wide-energy band gap and is a semiconductor. It will be used often in the next generation for 5G or satellites and further digitization and industrialization [3]. InN has the lowest mass for all electrons of all group-III semiconductors. This leads for the lowest saturation velocity and the highest mobility [4]. Concerning the elastic and mechanical properties of these materials, it is particularly relevant to analyze their behavior under pressure. This implies non linear elasticity effects to be very important.

In this work, we investigate the linear and non-linear elastic properties of boron nitride (BN), aluminum nitride (AlN), gallium nitride (GaN) and indium nitride (InN) in the zincblende structure. In addition, we investigate wurtzite AlN, too. The crystal structure and unit cell of these phases are shown in Figure 1.1. The goal of this work is twofold. Our first goal is to provide converged values of the second and third-order elastic constants and other elastic moduli calculated using state-of-the-art *ab-initio* methods. Secondly, we want to provide a benchmark for calculations of the elastic properties by analyzing explicitly the convergence with respect to the numerical parameters used in the calculations. Every calculation in this work is performed using density-functional theory (**DFT**) implemented in the software package **exciting** [5]. The calculations of the second and third-order elastic constants are performed using the **ElaStic** toolkit [6].

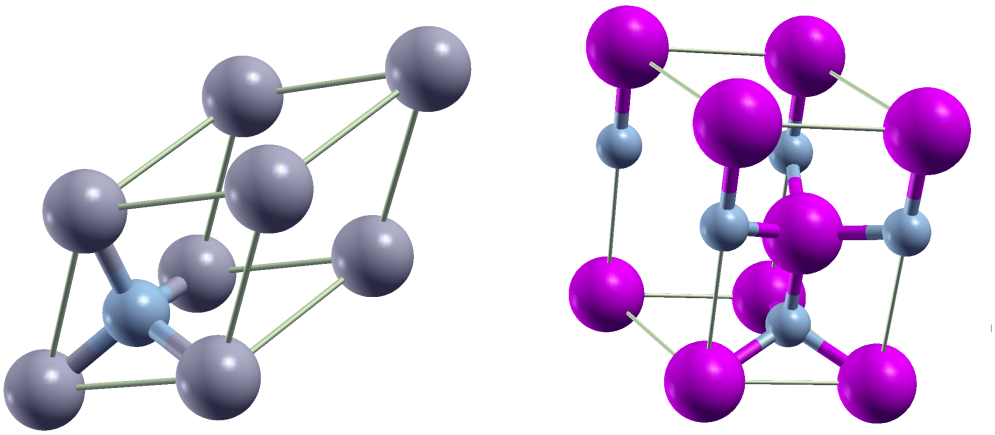

Figure 1.1: Crystal structure and unit cell of the cubic zincblende (left panel) and wurtzite (right panel) phase of group-III nitrides.

In addition, we analyze the possibility of using automatized workflows for the determination of elastic constants without explicit human intervention. To this purpose, we introduce the δ-parameter method, which can be used to automatize the interpretation of the polynomial fits for calculating finite-difference derivatives of the elastic energy.

Chapter 2

Theoretical background

This chapter provides a basic theoretical overview of the physical properties investigated in this thesis. We start by looking at the theory of the elasticity. Here, we give a deeper look at the elastic constants and moduli. Then, there is a short discussion about the energy of a quantum-mechanical system because the elastic constants are related to the change in energy of the system. Afterwords, we introduce density-functional theory (`DFT`) which allows to solve the quantum-mechanical problem for a crystal. In the last part of this chapter, we describe shortly the software package `exciting` [5] and the post-processing tool `ElaStic` [6].

2.1 Elasticity

In this section, we give a short introduction of the elastic properties of solid materials. A further discussion can be found in Refs. [6, 7, 8, 9]. If we apply external force on a solid material, the material experiences stress and with that a deformation. The movement of atoms to a new equilibrium position occurs because the internal forces try to cancel out the external forces. When the external forces and with that the stress is removed, the atoms move back to the initial equilibrium state and the deformation disappears. That is only possible if the stress was not too big and there was no rupture or fracture.

All the fundamental elastic quantities are introduced explicitly in the next sections, just after a short introduction on the notation we use to denote them.

2.1.1 Notation on naming matrices and vectors

Most of the physical quantities encountered in the elasticity theory are complex objects that cannot be simply expressed by a single scalar number. In this section, we introduce the notation we use throughout the thesis.

- A general vector in a 3-dimensional Cartesian space (*e.g.*, the position vector, see next section) is denoted by a single underlined symbol:

$$\underline{v} = (v_x, v_y, v_z)^{\mathrm{tr}} . \tag{2.1}$$

  where "tr" identifies the transpose operator and will be omitted in the next for the sake of simplicity.

- A general 3×3 matrix expressed in Cartesian indices (*e.g.*, strain and stress matrices, see next section) is denoted by a double underlined symbol:

$$\underline{\underline{a}} = \begin{pmatrix} a_{xx} & a_{xy} & a_{xz} \\ a_{yx} & a_{yy} & a_{yz} \\ a_{zx} & a_{zy} & a_{zz} \end{pmatrix} . \tag{2.2}$$

- A general vector in a 6-dimensional space (*e.g.*, the Voigt representation of strain and stress matrices, see the next sections) is denoted by a single underlined bold symbol:

$$\underline{\boldsymbol{\eta}} = (\eta_1, \eta_2, \eta_3, \eta_4, \eta_5, \eta_6) . \tag{2.3}$$

- A general matrix (6×6, 6×6×6, *etc.*) in a 6-dimensional space (*e.g.*, the Voigt representation of the elastic constants, see the next sections) is denoted by a double underlined bold symbol:

$$\underline{\underline{\boldsymbol{C}}} = \begin{pmatrix} C_{11} & C_{12} & C_{13} & C_{14} & C_{15} & C_{16} \\ C_{21} & C_{22} & C_{23} & C_{24} & C_{25} & C_{26} \\ C_{31} & C_{32} & C_{33} & C_{34} & C_{35} & C_{36} \\ C_{41} & C_{42} & C_{43} & C_{44} & C_{45} & C_{46} \\ C_{51} & C_{52} & C_{53} & C_{54} & C_{55} & C_{56} \\ C_{61} & C_{62} & C_{63} & C_{64} & C_{65} & C_{66} \end{pmatrix} . \tag{2.4}$$

  Notice that in later sections, this notation is generalized to any matrix in more than 3 dimensions.

2.1.2 Strain and stress

The state of deformation of a solid material can be described by the physical strain tensor $\underline{\underline{\epsilon}}$:

$$\underline{\underline{\epsilon}} = \begin{pmatrix} \epsilon_{xx} & \epsilon_{xy} & \epsilon_{xz} \\ \epsilon_{yx} & \epsilon_{yy} & \epsilon_{yz} \\ \epsilon_{zx} & \epsilon_{zy} & \epsilon_{zz} \end{pmatrix} . \tag{2.5}$$

Diagonal elements of the physical strain tensor signify deformations along the axes, whereas elements that are a combination of different positions describe shearing. From here now, we assume that all the discussed strain tensors are symmetric, *i.e.*, $\epsilon_{\alpha\beta} = \epsilon_{\beta\alpha}$. The tensor $\underline{\underline{\epsilon}}$ allows us to obtain the "strained" position of a point vector $\underline{r}$ in 3 dimension out of the "unstrained" one as

$$\underline{r}^{\text{strained}} = \underline{\underline{J}} \cdot \underline{r}^{\text{unstr.}} \equiv (\underline{\underline{1}} + \underline{\underline{\epsilon}}) \cdot \underline{r}^{\text{unstr.}} , \tag{2.6}$$

where $\underline{\underline{J}}$ and $\underline{\underline{1}}$ are the deformation and identity matrix, respectively. There are many types of strains for a crystal. In Figure 2.1 one can see some examples. Similarly,

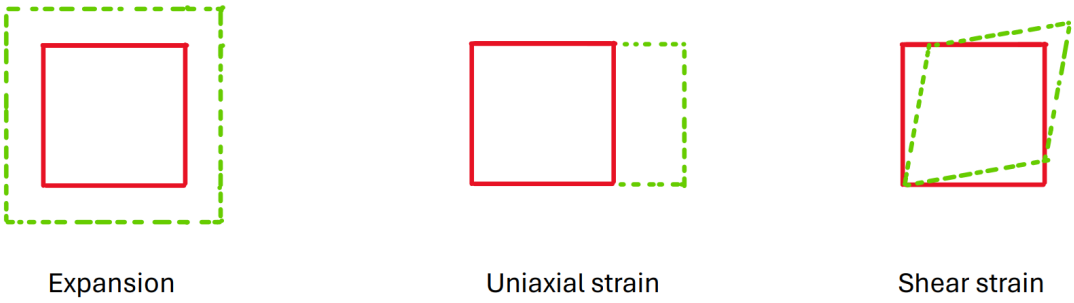

Figure 2.1: Examples of different strains in a two-dimensional space.

the stress tensor can also be written as

$$\underline{\underline{\sigma}} = \begin{pmatrix} \sigma_{xx} & \sigma_{xy} & \sigma_{xz} \\ \sigma_{yx} & \sigma_{yy} & \sigma_{yz} \\ \sigma_{zx} & \sigma_{zy} & \sigma_{zz} \end{pmatrix} , \tag{2.7}$$

where the single components, $\sigma_{\alpha\beta}$ are defined in terms of derivatives of the elastic energy, $E(\underline{\underline{\epsilon}})$, as:

$$\sigma_{\alpha\beta} = \frac{1}{V} \frac{\partial E(\underline{\underline{\epsilon}})}{\partial \epsilon_{\alpha\beta}} , \tag{2.8}$$

where V is the volume of the crystal.

In Ref. [10] it was shown that for treating non-linear elastic properties in a thermodynamically invariant way an alternative description of the strain is needed. For this reason, we introduce the Lagrangian strain tensor $\underline{\underline{\eta}}$:

$$\underline{\underline{\eta}} = \begin{pmatrix} \eta_{xx} & \eta_{xy} & \eta_{xz} \\ \eta_{yx} & \eta_{yy} & \eta_{yz} \\ \eta_{zx} & \eta_{zy} & \eta_{zz} \end{pmatrix} . \tag{2.9}$$

The Lagrangian strain tensor determines how the length of a general vector $\underline{v}$ changes during deformation:

$$\mid \underline{v}' \mid^2 - \mid \underline{v} \mid^2 = 2\underline{v} \cdot \underline{\underline{\eta}} \cdot \underline{v} \, . \tag{2.10}$$

The connection between the Lagrangian, $\underline{\underline{\eta}}$, and the physical, $\underline{\underline{\epsilon}}$, strain is given through the following relationship:

$$\underline{\underline{\eta}} = \underline{\underline{\epsilon}} + \frac{1}{2}\underline{\underline{\epsilon}}^2 \, . \tag{2.11}$$

It is important to notice that for small physical strain $\underline{\underline{\eta}} \approx \underline{\underline{\epsilon}}$.

A great simplification of the representations in the elasticity theory is provided by the Voigt notation, which we introduce in the next for the Lagrangian strain tensor $\underline{\underline{\eta}}$:

$$\begin{array}{lll} \eta_{xx} \rightarrow \eta_1 & \eta_{yy} \rightarrow \eta_2 & \eta_{zz} \rightarrow \eta_3 \\ \eta_{yz} + \eta_{zy} \rightarrow 2\eta_4 & \eta_{xz} + \eta_{zx} \rightarrow 2\eta_5 & \eta_{xy} + \eta_{yx} \rightarrow 2\eta_6 \, . \end{array}$$

Using the Voigt notation, the 3×3 matrix $\underline{\underline{\eta}}$ transforms into a 6-dimensional vector $\underline{\boldsymbol{\eta}}$.

2.1.3 Elastic constants

We can write the elastic energy of a material as a Taylor expansion in the Lagrangian strain $\underline{\boldsymbol{\eta}}$ as

$$E(\underline{\boldsymbol{\eta}}) = E_0 + \sum_i \sigma_i^{(0)} \, \eta_i + \frac{1}{2} \sum_{ij} C_{ij}^{(2)} \, \eta_i \, \eta_j + \frac{1}{6} \sum_{ijk} C_{ijk}^{(3)} \, \eta_i \, \eta_j \, \eta_k + ... \tag{2.12}$$

where $\underline{\underline{\boldsymbol{C}}}^{(2)}$ and $\underline{\underline{\boldsymbol{C}}}^{(3)}$ are the tensors of the second-order and third-order elastic constants in the Voigt notation, respectively. E_0 is the energy in the equilibrium (zero strain, zero force, ...) state of the crystal. $\underline{\boldsymbol{\sigma}}^{(0)}$ is the stress at equilibrium in the Voigt notation. The elastic constants of a given order are related to the

derivatives of the elastic energy of the corresponding order. Thus, with the second-order derivatives we obtain the second-order elastic constants (**SOECs**):

$$C_{ij}^{(2)} = \frac{1}{V} \frac{\partial^2 E(\underline{\boldsymbol{\eta}})}{\partial \eta_i \partial \eta_j}\bigg|_{\eta=0}. \tag{2.13}$$

In the Voigt notation, $\underline{\underline{\boldsymbol{C}}}^{(2)}$ is a 6×6 matrix:

$$\underline{\underline{\boldsymbol{C}}}^{(2)} = \begin{pmatrix} C_{11} & C_{12} & C_{13} & C_{14} & C_{15} & C_{16} \\ C_{21} & C_{22} & C_{23} & C_{24} & C_{25} & C_{26} \\ C_{31} & C_{32} & C_{33} & C_{34} & C_{35} & C_{36} \\ C_{41} & C_{42} & C_{43} & C_{44} & C_{45} & C_{46} \\ C_{51} & C_{52} & C_{53} & C_{54} & C_{55} & C_{56} \\ C_{61} & C_{62} & C_{63} & C_{64} & C_{65} & C_{66} \end{pmatrix}. \tag{2.14}$$

In the next, we omit the upper index (2), as it is sufficient to consider only the number of lower indices to identify the order of the elastic constants.

Because of the symmetry of the crystal, we can reduce the number of independent elastic constants. For example, the matrix of the second-order elastic constants for cubic systems is

$$\underline{\underline{\boldsymbol{C}}}^{(2)}_{\text{cubic}} = \begin{pmatrix} C_{11} & C_{12} & C_{12} & 0 & 0 & 0 \\ C_{12} & C_{11} & C_{12} & 0 & 0 & 0 \\ C_{12} & C_{12} & C_{11} & 0 & 0 & 0 \\ 0 & 0 & 0 & C_{44} & 0 & 0 \\ 0 & 0 & 0 & 0 & C_{44} & 0 \\ 0 & 0 & 0 & 0 & 0 & C_{44} \end{pmatrix}, \tag{2.15}$$

while the matrix for hexagonal (wurtzite) systems is

$$\underline{\underline{\boldsymbol{C}}}^{(2)}_{\text{hexagonal}} = \begin{pmatrix} C_{11} & C_{12} & C_{13} & 0 & 0 & 0 \\ C_{12} & C_{11} & C_{13} & 0 & 0 & 0 \\ C_{13} & C_{13} & C_{33} & 0 & 0 & 0 \\ 0 & 0 & 0 & C_{44} & 0 & 0 \\ 0 & 0 & 0 & 0 & C_{44} & 0 \\ 0 & 0 & 0 & 0 & 0 & \frac{(C_{11}-C_{12})}{2} \end{pmatrix}. \tag{2.16}$$

Furthermore, the third-order elastic constants (**TOECs**), $\underline{\underline{\boldsymbol{C}}}^{(3)}$, can be obteined in terms of the third-order derivatives of the elastic energy:

$$C^{(3)}_{ijk} = \frac{1}{V}\frac{\partial^3 E(\underline{\boldsymbol{\eta}})}{\partial\eta_i\partial\eta_j\partial\eta_k}\bigg|_{\eta=0}. \tag{2.17}$$

$\underline{\underline{\boldsymbol{C}}}^{(3)}$ is a 6×6×6 matrix with only 6 independent elastic-constants components for cubic system. These components are C_{111}, C_{112}, C_{123}, C_{144}, C_{155}, and C_{456}. The tensor of cubic (wurtzite) $\underline{\underline{\boldsymbol{C}}}^{(3)}$ is shown in the Appendix D (Appendix E).

2.1.4 Elastic moduli

We can connect the elastic constants to the mechanical properties of crystals in the Voigt notation by defining the following elastic muduli:

- **Shear modulus:**

$$G = \frac{1}{15}\Big[(C_{11}+C_{22}+C_{33}) - (C_{12}+C_{13}+C_{23}) + 3(C_{44}+C_{55}+C_{66})\Big]. \tag{2.18}$$

- **Bulk modulus:**

$$B_0 = \frac{1}{9}\Big[(C_{11}+C_{22}+C_{33}) + 2(C_{12}+C_{13}+C_{23})\Big]. \tag{2.19}$$

- **Young's modulus:**

$$E_{\rm Y} = \frac{9BG}{3B+G}\,. \tag{2.20}$$

- **Poisson ratio:**

$$\upsilon = \frac{3B-2G}{2(3B+G)}\,. \tag{2.21}$$

2.2 How to calculate the elastic energy

In order to perform an explicit calcuation of the elastic energy of a crystal introduced in the last section, one has to access the energy of a crystal out of the fundamental constituents (electrons and nuclei) and their (Coulomb) interactions. This task can be accomplished by using the quantum-mechanical expression for the *Total Energy* of a crystal seen as a system of electrons and nuclei. The concept of *Total Energy* and how it can be calculated in practice is discussed in the following sections.

2.2.1 Quantum mechanical energies

The full energy $\mathcal{E}$ of a system of $N \equiv N_{\text{elec}}$ electrons and N_{nuc} nuclei can be calculated by solving the full Schrödinger equation:

$$\hat{H}\,\Psi(r,R) = \mathcal{E}\,\Psi(r,R)\,, \tag{2.22}$$

where r denotes the set of positions of the electrons and is defined as $r = \{\underline{r}_i; i = 1,\ldots,N\}$. In the same way, R is the set of positions of the nuclei and is defined as $R = \{\underline{R}_I;\ I = 1,\ldots,N_{\text{nuc}}\}$. $\Psi(r,R)$ is the wave funcion and $\hat{H}$ is the Hamiltonian of the total system. $\hat{H}$ can be written as the following:

$$\hat{H} = \hat{T}_e + \hat{T}_n + \hat{V}_{nn} + \hat{V}_{ee} + \hat{V}_{ne}\,, \tag{2.23}$$

where $\hat{T}_e$ and $\hat{T}_n$ is the kinetic-energy operators of the electrons and nuclei and the operators $\hat{V}_{nn}$, $\hat{V}_{ee}$ and $\hat{V}_{ne}$ describe the Coulomb interactions between nuclei (index n) and electrons (index e). The full ground-state wave function can be written as

$$\Psi_{\text{GS}}(r,R) = \varphi_0(r,R)\,\chi_0(R)\,, \tag{2.24}$$

here, we use the Born-Oppenheimer (`BO`) approximation [11]. $\chi_0(R)$ is the nuclear wave functions and $\varphi_0(r,R)$ is the electronic wave functions. With the help of Eqs. (2.22) and (2.24) we can derive the following equation which only depends on the nuclear coordinates:

$$\hat{H}_{\text{BO}}\,\chi_0(R) = \left[\hat{T}_n + \hat{V}_{nn} + E_0(R)\right]\chi_0(R) = \mathcal{E}_{\text{BO}}\,\chi_0(R)\,, \tag{2.25}$$

where $\hat{T}_n$ is the operator for the kinetic energy of the nuclei and $\hat{V}_{nn}$ the potential between the nuclei. $E_0(R)$ is the ground-state energy of the electron system and H_{BO} is the nuclear Born-Oppenheimer Hamiltonian. It has an effective potential as the following:

$$U(R) = \hat{V}_{nn}(R) + E_0(R)\,. \tag{2.26}$$

We can calculate $E_0(R)$ by solving the following electronic equation:

$$\hat{H}_e\,\varphi_0(r;R) = \big[\hat{T} + \hat{W} + \hat{V}(R)\big]\varphi_0(r;R) = E_0(R)\,\varphi_0(r;R)\,. \tag{2.27}$$

$\hat{W}$ is the potential between the electrons, $\hat{V}$ represents the external nuclear potential acting on the electrons and $\hat{T}$ represents the kinetic energy for the electrons. In the following we focus on calculations of the energy of the crystal at a fixed nuclear configuration R. In this case, we can introduce what in the literature as usually called *Total Energy*, E_{tot}, by adding the constant term $\hat{V}_{nn}(R)$ to the electronic ground-state energy $E_0(R)$:

$$E_{\text{tot}} = E_0(R) + \hat{V}_{nn}(R)\,. \tag{2.28}$$

2.2.2 Density-functional theory

For the calculation of the elastic constants, we can identify the elastic energy with the total energy defined in Eq. 2.28. Because of the difficulty of the calculation of $E_0(R)$, we use the density-functional theory (`DFT`). This theory is discussed in this section.

`DFT` is based on the Hohenberg-Kohn (`HK`) theorem [12]. Hohenberg and Kohn were able to show that the total energy $E_{\text{tot}} \equiv E_{\text{GS}}$ in the ground state can be obtained by knowing the ground-state electron density $n_{\text{GS}}(\underline{r})$ only. This is because there is a one-to-one correspondence between every external potential $\hat{V}$ and its ground-state electron density $n_{\text{GS}}(\underline{r})$. Because of that every property of the system can be written as a functional of $n_{\text{GS}}(\underline{r})$. In particular, we get:

$$E_{\text{GS}} = E_{\text{GS}}[n_{\text{GS}}]. \tag{2.29}$$

Nevertheless, the `HK` theorem does not provide the explicit form of the functional in Eq. (2.29). Because of that, Kohn and Sham (`KS`) presented an approach which allows an easy calculation of the ground-state energy and electron density [13]. They showed that one can introduce a non-interacting single-particle system with the same ground-state electron density as the interacting many-body system. With the help of the `KS` approach, one can now write the ground-state energy functional as

$$\begin{aligned} E_{\text{GS}}[n] &= \langle \varphi_{\text{GS}}[n] \mid \hat{T} + \hat{W} + \hat{V} \mid \varphi_{\text{GS}}[n] \rangle \\ &= T_0[n] + E_{\text{H}}[n] + E_{\text{ext}}[n] + E_{\text{xc}}[n]\,, \end{aligned} \tag{2.30}$$

where $E_{\text{H}}[n]$ is the Hartree energy functional, $E_{\text{ext}}[n]$ is the energy functional corresponding to the external potential $\hat{V}$, $E_{\text{xc}}[n]$ is the (still unknown) exchange-correlation functional, and $T_0[n]$ represents the kinetic energy of the `KS` non-interacting system. The Hohenberg-Kohn theorem also states that $E_{\text{GS}}[n]$ is minimal for

$n = n_{\mathrm{GS}}$. Because of that, we can calculate n_{GS} by minimizing $E_{\mathrm{GS}}[n]$. This leads to the following equation:

$$\frac{\delta T_0[n]}{\delta n(r)} + v_{\mathrm{KS}}(r,[n]) = \mu_{\mathrm{chem}} \,, \tag{2.31}$$

where μ_{chem} is the chemical potential [14] and v_{KS} is the Kohn-Sham potential which is defined as:

$$\begin{aligned} v_{\mathrm{KS}}(\underline{r},[n]) &= \frac{\delta E_{\mathrm{H}}[n]}{\delta n(\underline{r})} + \frac{\delta E_{\mathrm{ext}}[n]}{\delta n(\underline{r})} + \frac{\delta E_{\mathrm{xc}}[n]}{\delta n(\underline{r})} \\ &= v_{\mathrm{H}}(\underline{r},[n]) + v_{\mathrm{ext}}(\underline{r}) + v_{\mathrm{xc}}(\underline{r},[n]) \,. \end{aligned} \tag{2.32}$$

The electron density which solve Eq. (2.31) is given as

$$n(\underline{r}) = \sum_{i=1}^{N} \mid w_i(\underline{r}) \mid^2 \,, \tag{2.33}$$

where the single-particle **KS** wave functions, $\{w_i(\underline{r})\}$, are the solution of the **KS** equations for the system of non-interacting particles:

$$\hat{h}_{\mathrm{KS}}(\underline{r})\, w_i(\underline{r}) \equiv \hat{h}(\underline{r})\, w_i(\underline{r}) = \left[-\frac{1}{2}\nabla^2 + v_{\mathrm{KS}}(\underline{r},[n]) \right] w_i(\underline{r}) = \varepsilon_i\, w_i(\underline{r}) \,. \tag{2.34}$$

Here, $\{\varepsilon_i\}$ are the single-particle **KS** energies.

Because $v_{\mathrm{KS}}(\underline{r},[n])$ itself is a function of the electron density $n(\underline{r})$, the **KS** equations must be solved self-consistently (see Figure 2.2). First, one take an initial guess for the electron density n. Then, the **KS** potential $v_{\mathrm{KS}}(\underline{r},[n])$ and the Hamiltonian $\hat{h}_{\mathrm{KS}}(\underline{r})$ are calculated by using the old electron density n. Solving the **KS** equations a new density can be calculated. Now we compare the new density with the old one and repeat this process until convergence is reached. This process is summarized in Figure 2.2.

Due to the fact that v_{xc} is not known exactly, one needs approximations for it. The most simple one is the local-density approximation (**LDA**) [13, 15]. Here v_{xc} is substituted locally with that of a homogeneous electron gas with a (local) electron density $n(\underline{r})$. Within **LDA**, one gets reasonable results for the total energies of metals, but it underestimates bond lengths. A better approximation than **LDA** is the generalized gradient approximation (**GGA**) [16]. It considers contributions from both the local electron density n and density gradient ∇n. **GGA** leads to better lattice parameters and total energies, nevertheless, band gaps are still underestimated. The most used **GGA** approximations are the one labeled as **PBE** [16] and **PBEsol** [17].

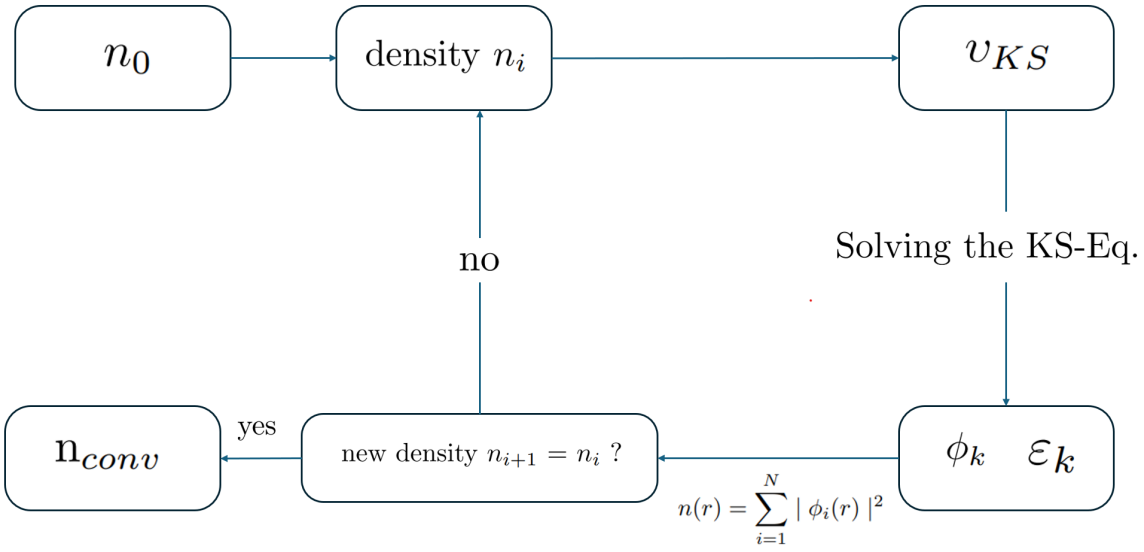

Figure 2.2: Scheme of a self-consistent cycle of a DFT-calculation.

2.2.3 Numerical solution of the Kohn-Sham equations

For a numerical solution of the self-consistent KS equations we use an expansion of the KS wave functions, $\{w_{i,\underline{k}}(\underline{r})\}$, in terms of a "known" set of basis functions, $\{\phi_{\nu,\underline{k}}(\underline{r})\}$:

$$w_{i,\underline{k}}(\underline{r}) = \sum_{\nu=1}^{\nu_{\max}} \gamma_{i,\underline{k}}^{\nu}\, \phi_{\nu,\underline{k}}(\underline{r})\,. \tag{2.35}$$

Here, due to the periodicity of the crystal, we have made explicit the dependence of the KS wave functions on the wave-vector index $\underline{k}$. Using the expansion in Eq. (2.35), the KS equations are transformed to a generalized matrix eigenvalue problem:

$$\left(\underline{\underline{\boldsymbol{h}}}(\underline{k}) - \varepsilon_{i,\underline{k}}\, \underline{\underline{\boldsymbol{s}}}(\underline{k})\right) \cdot \underline{\boldsymbol{\gamma}}_{\underline{k}} = 0\,. \tag{2.36}$$

Where $\underline{\boldsymbol{\gamma}}_{\underline{k}}$ is the vector of the unknown coefficients in Eq. (2.35), $\underline{\underline{\boldsymbol{s}}}(\underline{k})$ is the overlap matrix with components

$$s_{\nu,\mu}(\underline{k}) = \langle \phi_{\nu,\underline{k}} \mid \phi_{\mu,\underline{k}} \rangle\,, \tag{2.37}$$

and $\underline{\underline{\boldsymbol{h}}}_{\underline{k}}$ is the matrix representation in the $\{\phi_{\nu,\underline{k}}(\underline{r})\}$ basis of the single-particle KS hamiltonian with components

$$h_{\nu,\mu}(\underline{k}) = \langle \phi_{\nu,\underline{k}} \mid \hat{h} \mid \phi_{\mu,\underline{k}} \rangle\,. \tag{2.38}$$

The choice of the basis functions must be careful because the KS wave functions strongly vary close to the nuclei. In this work, the numerical solution of the KS equations is performed as implemented in the **exciting** code which is described in the next section.

2.3 The software package exciting

The software package **exciting** [5] is here used to calculate the total energy of a crystal for given nuclear configurations. **exciting** is a full-potential all-electron **DFT** package implementing linearized augmented planewave methods. Its big advantage with respect to other *ab-initio* codes is that in **exciting** core electrons are explicitly treated without the use of a pseudo-potential.

2.3.1 Basis functions in exciting

The **exciting** code utilizes a basis set consisting of linearized augmented plane waves (**LAPWs**) and local orbitals. The unit-cell volume is divided into muffin-tin (**MT**) and interstitial (**I**) regions. The **MT** regions are spheres with the radius R_{MT} which are centered around the atoms with the position $\underline{R}_\alpha$. The **MT** wave functions present strong oscillation in the **MT** regions while their variation in the interstitial region is quite soft. In order to represent at best this behaviour, **exciting** uses as basis functions the augmented plane waves (**APWs**):

$$\phi^{\mathrm{APW}}_{\underline{k}+\underline{G}}(\underline{r}) = \begin{cases} \sum_{lm} A^{\underline{k}+\underline{G}}_{lm\alpha}\, u_{l\alpha}(r_\alpha)\, Y_{lm}(\hat{\underline{r}}_\alpha)\,, & r_\alpha \le R_{\mathrm{MT}} \\ \frac{1}{\sqrt{V}}\, \mathrm{e}^{i(\underline{k}+\underline{G})\cdot\underline{r}}, & \underline{r} \in \mathrm{I}\,, \end{cases} \tag{2.39}$$

where $\underline{G}$ is a reciprocal lattice vector and $\underline{r}_\alpha = \underline{r} - \underline{R}_\alpha$. In the **MT** region, $Y_{lm}(\hat{\underline{r}}_\alpha)$ are the spherical harmonics, $u_{l\alpha}(r_\alpha)$ are radial functions and $A^{\underline{k}+\underline{G}}_{lm\alpha}$ are chosen such that $\phi^{\mathrm{APW}}_{\underline{k}+\underline{G}}(\underline{r})$ are continuous at the boundary of the **MT** spheres. In the interstitial region, the **APW** is a simple plane wave.

An alternative to the **APWs** are the linear augmented plane waves (**LAPWs**). The basis function for the interstitial part does not change, but the **MT** part is now written as

$$\phi^{\mathrm{LAPW}}_{\underline{k}+\underline{G}}(\underline{r}) = \sum_{lm} \left[A^{\underline{k}+\underline{G}}_{lm\alpha}\, u_{l\alpha}(r_\alpha;\varepsilon_{l\alpha}) + B^{\underline{k}+\underline{G}}_{lm\alpha}\, \dot{u}_{l\alpha}(r_\alpha);\varepsilon_{l\alpha} \right] Y_{lm}(\hat{\underline{r}}_\alpha)\,, \tag{2.40}$$

where $\dot{u}_{l\alpha}$ is the energy derivative of the radial function $u_{l\alpha}$ and $B^{\underline{k}+\underline{G}}_{lm\alpha}$ is determined such that the derivative of the basis function is also continuous at the boundary of the **MT** spheres.

In addition to the (**L**)**APWs**, **exciting** uses local orbitals (**LOs**) in the set of basis functions. The **LOs** vanish inside the interstitial region. In the **MT** region, we have:

$$\phi^{\mathrm{LO}}_{\mu}(\underline{r}) = \delta_{\alpha\alpha_\mu}\, \delta_{ll_\mu}\, \delta_{mm_\mu} \left[a_\mu\, u_{l\alpha}(r_\alpha;\varepsilon_{l\alpha}) + b_\mu\; u_{l\alpha}(r_\alpha;\varepsilon_{l\alpha}) \right] Y_{lm}(\hat{\underline{r}}_\alpha). \tag{2.41}$$

The coefficients a_μ and b_μ make the **LO** normalized and vanishing at the **MT** boundary.

By including both **LOs** and **APWs**, the **KS** wave function can be written as:

$$w_{i,\underline{k}}(\underline{r}) = \sum_{\underline{G}} \gamma^{\mathrm{APW}}_{\underline{k}+\underline{G}}\, \phi^{\mathrm{APW}}_{\underline{k}+\underline{G}}(\underline{r}) + \sum_{\mu} \gamma^{\mathrm{LO}}_{\mu}\, \phi^{\mathrm{LO}}_{\mu}(\underline{r})\,. \tag{2.42}$$

To keep the basis set size finite, we limit the values of $|\underline{k}+\underline{G}|$ with a maximum cut-off value $G_{\max}$ and with finite number of local orbitals. In **exciting**, the size of the **APW** basis-function set is given by fixing the parameter $R^{\min}_{\mathrm{MT}}\, G_{\max}$ (**rgkmax** in the input file). Here, $R^{\min}_{\mathrm{MT}}$ is the smallest muffin-tin radius in the unit-cell.

2.3.2 Brillouin-zone sampling

In order to calculate the total energy within **DFT**, one has to perform integrations over the first Brillouin zone of the crystal of quantities which are expensive to be calculated. This problem is generally solved in **DFT** codes by approximating the integrals by sum performed over discrete $\underline{k}$-grid meshes. In **exciting**, the used mesh is defined by the parameter(s) **ngridk** consisting of three non-vanishing natural numbers each of them indicating the density of $\underline{k}$-points along the basis vectors in reciprocal space.

2.4 The ElaStic tool

The **ElaStic** tool [6] allows for the *ab-initio* calculation of the full second-order (**SOECs**) and third-order (**TOECs**) elastic constants for materials with a variety of crystal structures.

Figure 2.3 shows the process of the calculation of elastic constants. First, the available computer package for the **DFT** calculation is chosen. In this work, all calculations are performed using **exciting**. In the next step, the input file for the equilibrium configuration with information on the structure (atomic positions, crystal lattice, *etc.*) is read by **ElaStic**. Then, the space-group number is determined by the program **SGROUP**. Thus, **ElaStic** has now a complete characterization of the system. With the knowledge of the space-group number, **ElaStic** now specifies deformation types.

The user gives two input values. The first value, $\eta^{(\mathtt{ElaStic})}_{\max}$, is the absolute value of the maximum Lagrangian strain. The second value is the number of the distorted structures for each deformation type in the range $-\eta^{(\mathtt{ElaStic})}_{\max}$ to $\eta^{(\mathtt{ElaStic})}_{\max}$. After that, for every deformed structure an input file is created. **DFT** calculations are performed including for each nuclear configuration the optimization of the internal degrees of freedom.

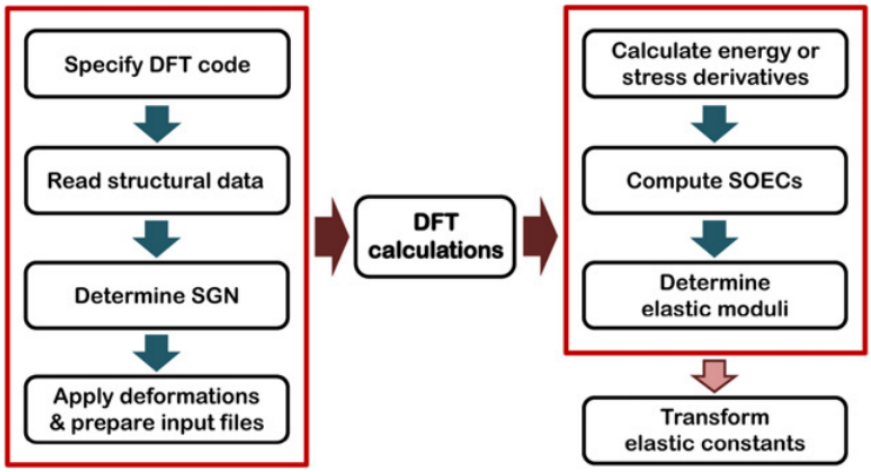

Figure 2.3: Flowchart of the process used in `ElaStic` (from Ref. [6]).

After the calculation, the total energy of the selected deformed structures is available. According to the definitions given in Eqs. (2.13) and (2.17) the elastic constants are given in terms of derivatives of the total energy with respect to the lagrangian strain. In order to calculate these derivatives the energy-versus-strain curves are fitted with polynomials of different orders. Then, the derivatives are calculated analytically from the expression of the fitting polynomials. However, the results which are obtained following this procedure are strongly dependent on the fitting range. In order to extract out of the fit the optimal value of these derivatives, a "plateau" value must be identified [6]. This requires some human "eye" intervention. Finding a method to circumvent this disadvantage is among the goals of this work, as we discuss in the next chapters. Finally, the elastic moduli can be obtained as defined in Section 2.1.4.

Chapter 3

Results

In this chapter, we present and discuss the results of our calculations. First, we describe the computational parameters used in the calculations. Then, we briefly show the obtained structural properties for the equilibrium state of the group-III nitrides. For these materials, we evaluate the second and third-order elastic constants for different sets of values of the computational parameters. In addition, we introduce a method for optimizing the calculation of energy derivatives by means of polynomial fits and show, how this procedure affect the values of the elastic constants. Then, the converged values of the elastic constants are compared with the experimental and theoretical values available in the literature. Finally, the results for the different materials are analyzed in order to establish trends.

3.1 Computational details

All calculations presented here are performed using **DFT** as implemented in the **exciting** code. For the exchange-correlation energy functional, we use the generalized gradient approximation (**GGA**), in the **PBE** [16] and **PBEsol** [17] approaches. In particular, the **PBEsol** functional is taylored to improve the determination of equilibrium properties of densely packed solids [16]. We use species files from Ref. [18].

The following set of computational parameters are responsible of the accuracy in the evaluation of ground-state properties using **exciting**. In the following, we use for these parameters a notation as given in the "Input Reference" of the **exciting** code [19]. The first important parameter is **rgkmax** which determines the number of basis functions used for the calculation and is defined as $R_{\mathrm{MT}}^{\mathrm{min}} \, |\underline{k} + \underline{G}|_{\mathrm{max}}$ (see Section 2.3.1). The next parameter is **ngridk**, a set of three integers, which determines the number of $\underline{k}$-points along the directions of the basis vectors. As next, **gmaxvr** is the maximum length of the reciprocal lattice vectors for expanding the interstitial

```
<input>

   <title>AlN</title>

   <structure speciespath="...">
      <crystal scale="8.2757">
         <basevect> 0.5     0.5     0.0 </basevect>
         <basevect> 0.5     0.0     0.5 </basevect>
         <basevect> 0.0     0.5     0.5 </basevect>
      </crystal>
      <species speciesfile="Al.xml" rmt="1.50">
         <atom coord="0.00 0.00 0.00" />
      </species>
      <species speciesfile="N.xml" rmt="1.40">
         <atom coord="0.25 0.25 0.25" />
      </species>
   </structure>

   <groundstate
      ngridk="12 12 12"
      swidth="0.0001"
      gmaxvr="25"
      rgkmax="9"
      lmaxapw="12"
      lmaxvr="12"
      xctype="GGA_PBE_SOL">
   </groundstate>

   <relax/>

</input>
```

Figure 3.1: Example of the input file of an **exciting** calculation for AlN.

density and potential. The last parameters we consider in this work are **lmaxvr** and **lmaxapw** which are the angular momentum cut-off used for the hamiltonian and overlap matrix setup and for the augmented plane wave functions, respectively. Figure 3.1 shows an example input file which contains these parameters.

In order to further simplify the denomination of the computational parameters used in our calculation, we use from now on the shortened notation reported in Table 3.1. Using this notation, the computational parameters used in a calculation can be summarized in a single string, *e.g.*, "**r8.k8.g12.l8**" means that **rgkmax** is set to "8", **ngridk** to "8 8 8", **gmaxvr** to "12", as well as **lmaxvr** and **lmaxapw** are set to "8".

Table 3.1: Notation used in this thesis for the denomination of the most important computational parameters of the **exciting** code.

parameter(s) in **exciting**	short cut
rgkmax	**r**
nkgrid (cubic)	**k**
gvrmax	**g**
lmaxvr **lmaxapw**	**l**

For materials in the zincblende structure different sets of values of these parameters have been used. At variance, we employed for the calculation of wurtzite AlN a fixed set of values (shown in Table 3.2), due to time issues.

Table 3.2: Chosen parameters and values for AlN in the wurtzite structure.

rgkmax	9
ngridk	12×12×8
gmaxvr	16
lmaxvr/lmaxapw	8

3.2 Structural properties

In this section, we give the results for the calculated lattice parameter and bulk modulus for the equilibrium configuration. Later, these values are used for the calculation of the elastic constants.

The equilibrium parameters are calculated according to the following procedure. Starting from an initial non-equilibrium value of the lattice parameter, we performed calculations of the total energy for a series of distorted structures where only the lattice parameter a is changed in a range of positive and negative variations. Using a similar approach to the one explained in the next section for obtaining the energy derivatives, the lattice parameter which minimize the total energy has been obtained. In a second step, the procedure is repeated by using as reference the equilibrium lattice parameter determined in the first step. The second derivative of the energy calculated at equilibrium gives us the value of the equilibrium bulk modulus B_0, multiplied by the number 9. Of course this procedure is valid only for the cubic structures with only one structural degree of freedom. For the wurtzite structure the lattice parameters are determined in a similar way by minimizing the total energy with respect to both the a and c parameters.

An example showing the calculated total energy as a function of a "volume" strain changes is given below in Figure 3.2. The values of the computational parameters used for converged calculation of the structural properties of our zincblende materials are given in the "string" notation as `r9.k12.g25.l12`. For the AlN in the wurzite structure we used the values given in Table 3.2. The converged result for the equilibrium parameters is shown in Tables 3.3 to 3.7.

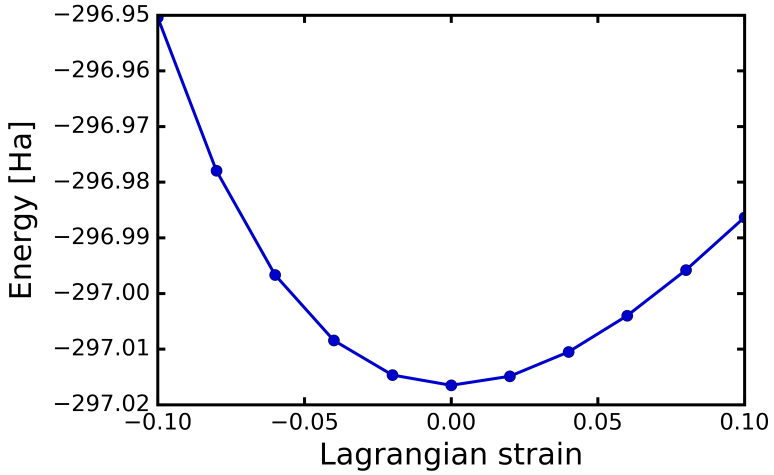

Figure 3.2: Calculated energy (blue solid circles) as a function of the lagrangian strain corresponding to a homogeneous volume deformation for AlN in the zincblende structure.

Table 3.3: Lattice constant a and bulk modulus B_0 of BN.

BN	Ref.	E_{xc}	a [Å]	B_0 [GPa]
Present work		**PBE**	3.6256	371.3
		PBEsol	3.6066	385.3
Theory	[20]	**PBE**	3.63	374
	[21]	**GGA**	3.63	380
	[22]	**GGA**	3.615	362
	[23]	**LDA**	3.59	400
Experiment	[29]		-	400
	[24]		3.6157	381.1
	[25]		3.615	-

Table 3.4: Lattice constant a and bulk modulus B_0 of AlN.

AlN	Ref.	E_{xc}	a [Å]	B_0 [GPa]
Present work		**PBE**	4.4057	191.4
		PBEsol	4.3793	199.3
Theory	[23]	**LDA**	4.32	203
	[26]	**HSE**	4.3647	-
	[21]	**GGA**	4.40	211
	[27]	**PBE**	4.38	195.5
Experiment	[28]		4.38	-
	[29]		4.373	-

Table 3.5: Lattice constant, a, and bulk modulus, B_0, of GaN.

GaN	Ref.	E_{xc}	a [Å]	B_0 [GPa]
Present work		`PBE`	4.5554	169.3
		`PBEsol`	4.5044	185.9
Theory	[20]	`PBE`	4.51	172
	[26]	`HSE`	4.4925	-
	[30]	`GGA`	4.582	162.2
	[30]	`LDA`	4.461	199.1
Experiment	[31]		4.54	-
	[32]		4.510	-
	[33]		4.49	-
	[34]		4.506	-

Table 3.6: Lattice constant a and bulk modulus B_0 of InN.

InN	Ref.	E_{xc}	a [Å]	B_0 [GPa]
Present work		`PBE`	5.0645	121.3
		`PBEsol`	5.0022	136.3
Theory	[26]	`HSE`	4.9908	-
	[23]	`LDA`	4.92	139
Experiment	[35]		4.98	-
	[36]		5.01	-

Table 3.7: Lattice constant a and c and bulk modulus B_0 of wurtzite AlN.

AlN	Ref.	E_{xc}	a [Å]	c [Å]	B_0 [GPa]
Present work		`PBEsol`	3.1147	4.9867	-
Theory	[23]	`LDA`	3.06	4.91	202
	[37]	`LDA`	3.100	4.964	209
	[38]	`LDA`	-	-	210.3
	[38]	`GGA`	-	-	185.4

3.3 Elastic properties

In this section, we present the results of the calculation of the second (**SOECs**) and third-order (**TOECs**) elastic constants for the group-III nitrides. In the following, we describe the steps we followed for performing these calculations using the **ElaStic** tool.

3.3.1 Using ElaStic for calculating elastic constants

- **Step 1: Generate distortions**

  In the first step **ElaStic** generate input files for **exciting** for different distortion types and different strain amplitudes in the range $[-\eta_{\max}^{(\texttt{ElaStic})}, \eta_{\max}^{(\texttt{ElaStic})}]$ depending on the symmetry of the starting equilibrium structure. The distortion types used by **ElaStic** for the zincblende (wurtzite) structure are shown in Table 3.8 (Table 3.10) for the **SOECs** and Table 3.9 (Table 3.11) for the **TOECs**, respectively.

Table 3.8: Distortion types used by **ElaStic** for cubic systems and **SOECs**.

Distortion	η_1	η_2	η_3	η_4	η_5	η_6
Dst01	η	η	η	0	0	0
Dst02	η	η	0	0	0	0
Dst03	0	0	0	2η	2η	2η

Table 3.9: Distortion types used by **ElaStic** for cubic systems and **TOECs**.

Distortion	η_1	η_2	η_3	η_4	η_5	η_6
Dst01	η	η	η	0	0	0
Dst02	η	η	0	0	0	0
Dst03	0	0	0	2η	2η	2η
Dst04	η	η	$-\eta$	0	0	0
Dst05	η	0	0	2η	0	0
Dst06	η	0	0	0	2η	0

Table 3.10: Distortion types used by **ElaStic** for wurtzite systems and **SOECs**.

Distortion	η_1	η_2	η_3	η_4	η_5	η_6
Dst01	η	η	η	0	0	0
Dst02	$0.5\,\eta$	$0.5\,\eta$	$-\eta$	0	0	0
Dst03	0	0	η	0	0	0
Dst04	0	η	0	0	0	0
Dst05	0	0	η	$2\,\eta$	0	0

Table 3.11: Distortion types used by **ElaStic** for wurtzite systems and **TOECs**.

Distortion	η_1	η_2	η_3	η_4	η_5	η_6
Dst01	η	η	η	0	0	0
Dst02	$0.5\,\eta$	$0.5\,\eta$	$-\eta$	0	0	0
Dst03	0	0	η	0	0	0
Dst04	0	η	0	0	0	0
Dst05	0	0	η	$2\,\eta$	0	0
Dst06	$0.5\,\eta$	$0.5\,\eta$	$-\eta$	0	0	$2\,\eta$
Dst07	η	η	0	0	0	0
Dst08	η	0	0	0	0	0
Dst09	η	0	0	$2\,\eta$	0	0
Dst10	0	η	0	$2\,\eta$	0	0

- **Step 2: Energy data vs. strain values**

  For each input file, an **exciting** calculation is performed and the corresponding total energy is extracted. Then, for a given distortion type a curve of total energy as a function of the strain amplitude is obtained, *e.g.*, as shown in Figure 3.2.

- **Step 3: Polynomial fits**

  At this step, a fit of the energy-vs.-strain curves is performed using polynomials of order $n = 2, 4, 6$ ($n = 3, 5, 7$) for the **SOECs** (**TOECs**). This procedure is repeated including calculated points corresponding to different symmetric strain ranges in the form $[-\eta_{\rm max}^{\rm (fit)}, \eta_{\rm max}^{\rm (fit)}]$. In the next, we set $\eta_{\rm max}^{\rm (fit)} \equiv \eta_{\rm max}$.

- **Step 4: Extract energy derivatives: The "human-eyes" problem**

  Energy derivatives are calculated analytically for the polynomials obtained in the previous step. The results for these derivatives as a function of the used range of strains (here indicated by the value of $\eta_{\max}$="maximum lagrangian strain") are summarized in plots similar to those shown in Figures 3.3 and 3.4. The difference between the results shown in Figures 3.3 and 3.4 is that in the first case (Figure 3.3) the used computational parameters (in particular for **`rgkmax`** and **`ngridk`**) provide a poor description of the **`KS`** wave functions while this description is very accurate for the choice of parameters in the second case (Figure 3.4). In this last case, a "plateau" of the represented curves is very easy to be identified with high accuracy. The same is not true for Figure 3.3. As stated in Ref. [6], the value which corresponds to this "plateau" is the best possible value for the energy derivative according to the polynomial fit.

  Up to now, the recognition of the position and value of the "plateau" of the energy derivatives was left by **`ElaStic`** to "human-eyes", assuming the user to check on the plots these values. Of course, this represents a problem in view of a fully automatized calculation of converged elastic constants by means of generals workflows.

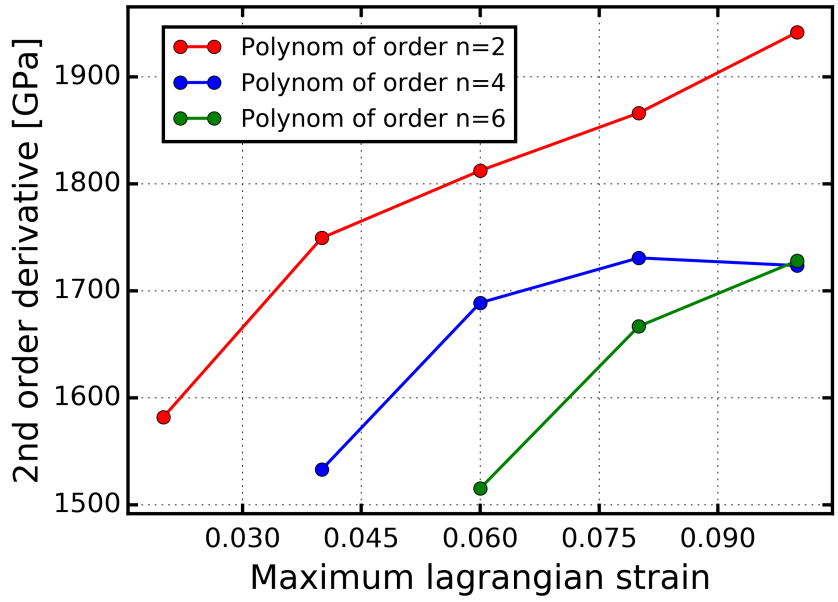

Figure 3.3: Dependence of the calculated energy-per-volume derivatives on the maximum lagrangian strain used in the fitting procedure. The parameters used in the calculations are **`r6.k8.g12.18`**.

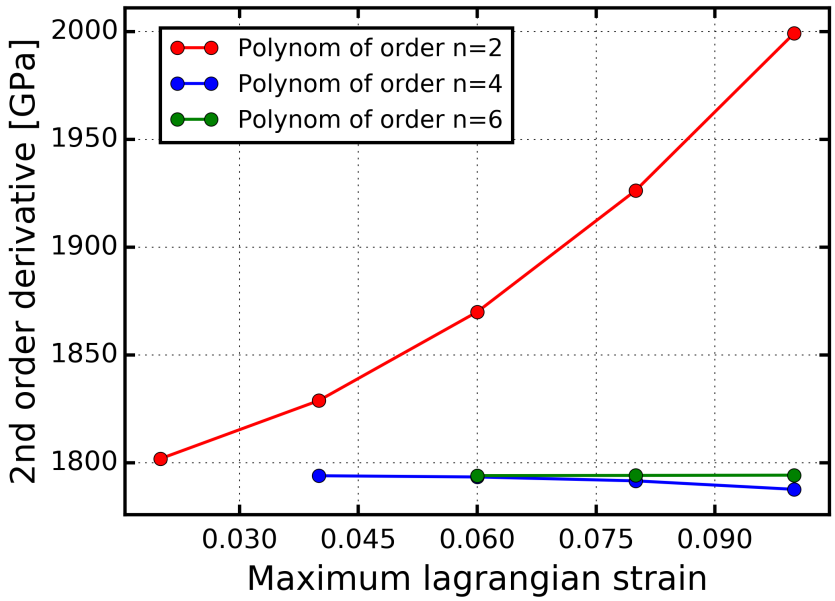

Figure 3.4: Dependence of the calculated energy-per-volume derivatives on the maximum lagrangian strain used in the fitting procedure. The parameters used in the calculations are `r9.k12.g25.l12`.

3.3.2 How to overcome the "human-eyes" problem

In the following, we present a method to overcome the "human-eyes" problem.

The δ-parameter method

First, we choose a range $[\eta_{\max}^{(\text{left})}, \eta_{\max}^{(\text{right})}]$ for the values of $\eta_{\max}$ used for the polynomial fit (see *e.g.*, Figure 3.5). Then, the value of the parameter δ is defined by the difference between the highest and lowest value of the energy derivative in this range in correspondence to the highest polynomial order used for the fit. The value of the parameter δ which is obtained in this way represents a measure of the accuracy of the fit procedure for the determination of the energy derivative. Figure 3.5 shows the situation for not fully optimized computational parameters, in particular the value of **`gmaxvr`** is here set to "18". The corresponding δ-parameter has a value of about 0.6 GPa. A much better value of δ can be obtained by increasing **`gmaxvr`** to the value "25", which provides a value of at least an order of magnitude smaller, as can be seen in Figure 3.6. At variance, the analysis which we performed indicates that the contemporary increase of the values of **`lmaxvr`** and **`lmaxapw`** has only a very small influence on the value of the δ-parameter.

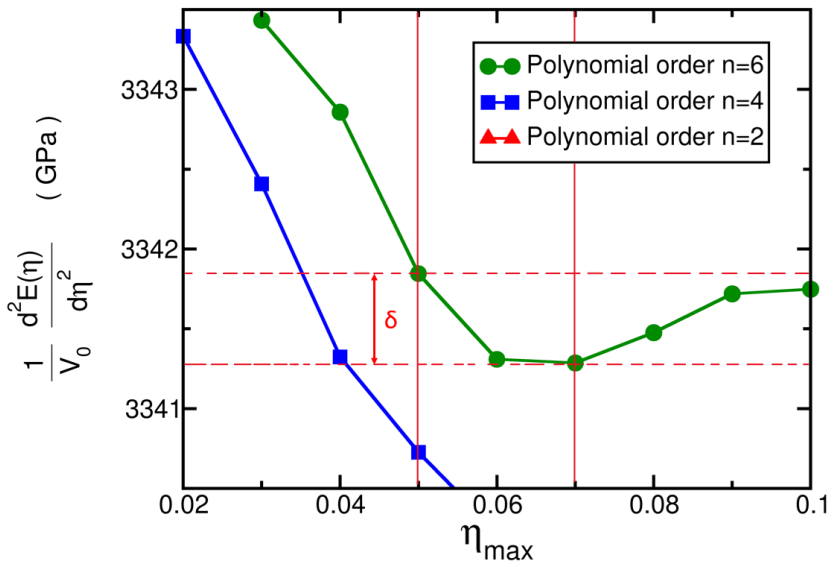

Figure 3.5: Identification of the plateau region of the second-order energy derivatives performed with the δ-parameter method for `Dst01` of zincblende BN with parameters `r9.k12.g18.l8`. Here, the vertical (red) solid lines correspond to the values of $\eta_{max}^{(left)}$ (left line) and $\eta_{max}^{(right)}$ (right line).

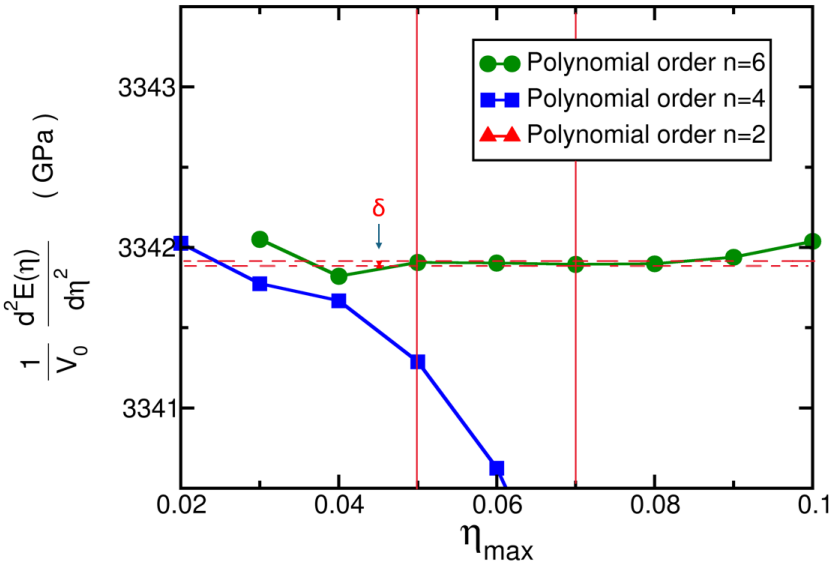

Figure 3.6: Same as Figure 3.5 with `gmaxvr`="25".

Table 3.12: Range $\left[\eta_{\max}^{(\text{left})}, \eta_{\max}^{(\text{right})}\right]$ used for the analysis of the energy derivatives obtained from the polynomial fits for the zincblende materials.

Material		$\eta_{\max}^{(\text{left})}$	$\eta_{\max}^{(\text{right})}$	Distortion(s)
BN	`SOECs`	0.05 0.04	0.07 0.06	`Dst01`,`Dst02` `Dst03`
AlN	`SOECs`	0.05	0.07	`Dst01-Dst03`
GaN	`SOECs`	0.05	0.07	`Dst01-Dst03`
InN	`SOECs`	0.05	0.07	`Dst01-Dst03`
BN	`TOECs`	0.05 0.04	0.07 0.06	`Dst01-Dst06` `Dst03`
AlN	`TOECs`	0.06	0.08	`Dst01-Dst06`
GaN	`TOECs`	0.05	0.07	`Dst01-Dst06`
InN	`TOECs`	0.05	0.07	`Dst01-Dst06`

In this work, we used for the range $[\eta_{\max}^{(\text{left})}, \eta_{\max}^{(\text{right})}]$ the values indicated in Table 3.12. As an example, the values of the δ-parameter calculated for each deformation used in the determination of `SOECs` (`TOECs`) of zincblende AlN using are shown in Table 3.13 (Table 3.14). Tables for all materials are shown in Appendix A. From the analysis of these tables, we can see that in most cases the higher the values for the parameters are set, the smaller is the value of δ. For example, in Table 3.13 the smallest value of δ is obtained for the parameters `r9.k12.g25.l12` in `Dst01` and `Dst02`,

Table 3.13: Values of the δ-parameter in units of [GPa] for the second-order energy derivatives of zincblende AlN using `PBEsol`.

`r`	`k`	`g`	`l`	`Dst01`	`Dst02`	`Dst03`
8	8	12	8	3.07	1.83	1.51
8	8	25	12	2.05	1.25	1.07
8	12	12	8	2.24	1.62	0.58
8	12	25	12	0.59	0.19	0.16
9	8	25	12	0.38	0.31	0.04
9	12	16	8	0.37	0.53	0.14
9	12	25	12	0.07	0.03	0.19

Table 3.14: Same as Table 3.13 for third-order energy derivatives.

r	k	g	l	Dst01	Dst02	Dst03	Dst04	Dst05	Dst06
8	8	12	8	524	753	352	169	496	331
8	8	25	12	62	108	29	46	46	40
8	12	12	8	618	607	305	229	438	329
8	12	25	12	36	38	44	38	11	20
8	16	12	8	678	597	304	189	404	311
9	8	25	12	11	38	22	3	15	9
9	12	16	8	50	16	43	10	5	16
9	12	25	12	6	11	11	3	1	1

but not for **Dst03**. However, the overall trend, also for **Dst03**, is very clear. As a general statement, the parameters **rgkmax** and **ngridk** have obviously a big influence on the convergence. This is shown in Table 3.13. Analyzing the combinations **r8.k8.g25.l12** and **r8.k12.g12.l8** in Table 3.14, one can see that even if **ngridk** is increased, the lower valuer of **gmaxvr** leads to much larger values of δ. Overall, the values of the δ-parameter are much higher for **TOECs** than for **SOECs**, as one might expect due to the higher order of numerical derivation.

In the next, we use the following notation for classifying the calculations of the elastic constants performed using **ElaStic**:

EYE denotes all calculations which are performed using the "human-eyes" intervention for identifying the best "plateau" value for the energy derivatives.

STD is used if the identification of the "plateau" value is performed using a fixed value $\eta_{\max} = 0.07$, which turned to be the "suggested value" from the analysis performed with the δ-parameter method introduced in this section.

3.3.3 Benchmark data for different parameter settings

In this work, we provide *ab-initio* calculations of the elastic constants of group-III nitrides for several sets of values of computational parameters. The full results can be found in Appendix B. These calculations represent a benchmark for analysing the convergence of both **SOECs** and **TOECs** of these materials. In this section, we focus on the results concerning zincblende AlN calculated using **PBE**, that are shown in Tables 3.15 and 3.16 for the **SOECs** and **TOECs**, respectively.

When using the **ElaStic** tool for calculating the elastic constants of a material, one has to consider two main convergence behaviours. The first is related to the convergence of the values of the elastic constants directly with respect to the computational parameters. This can be extracted by analysing Tables 3.15 and 3.16. Secondly, one has to consider the convergence of the numerical energy derivatives with respect to the fit parameters. This information can be obtained by analysing the results of the δ-parameter shown in Tables 3.13 and 3.14. Including both considerations, we can argue that for this material the elastic data obtained for the numerical parameters **r9.k12.g25.l12** are converged up to 0.1 GPa for the **SOECs** and from 1 to 10 GPa for **TOECs** (depending on the distortion type).

Table 3.15: **SOECs** of AlN in units of [GPa] calculated using **PBEsol**, only results obtained using the **EYE** method are included.

r	**k**	**g**	**l**	C_{11}	C_{12}	C_{44}
8	8	12	8	284.8	156.9	178.6
8	8	25	12	285.2	156.5	178.6
8	12	12	8	285.6	156.1	178.5
8	12	25	12	285.3	156.4	178.5
9	8	25	12	285.3	156.4	178.5
9	12	16	8	285.5	156.3	178.5
9	12	25	12	285.3	156.4	178.4

Table 3.16: Same as Table 3.15 for the **TOECs** of AlN in units of [GPa].

r	**k**	**g**	**l**	C_{111}	C_{112}	C_{123}	C_{144}	C_{155}	C_{456}
8	8	12	8	-1094	-999	-51	53	-718	3
8	8	25	12	-1073	-989	-53	58	-718	1
8	12	12	8	-1143	-980	-35	58	-722	3
8	12	25	12	-1051	-980	-47	57	-721	1
9	8	25	12	-1044	-980	-46	57	-721	2
9	12	16	8	-1061	-979	-46	56	-721	1
9	12	25	12	-1050	-980	-46	57	-720	1

3.3.4 Elastic constants of zincblende group-III nitrides

In this section, we show the converged values of the elastic constants calculated for the zincblende nitrides. When available, our results are compared with previously published theoretical and experimental values. As an example, the **SOECs** and **TOECs** of zincblende AlN are presented in Tables 3.17 and 3.18, respectively. Tables containing our values of the elastic constants for all zincblende nitrides can be found in Appendix C.

Table 3.17: **SOECs** of zincblende AlN in units of [GPa].

AlN	Ref.	E_{xc}		C_{11}	C_{12}	C_{44}
Present work		**PBE**	**EYE**	279.7	147.2	176.9
		PBE	**STD**	279.8	147.2	176.9
		PBEsol	**EYE**	285.3	156.4	178.4
		PBEsol	**STD**	285.3	156.4	178.4
Theory	[39]	**PBE**		284	167	181
	[20]	**PBE**		283	150	180
	[27]	**PBE**		315	130	245
	[26]	**HSE**		309.5	166.1	196.9
	[21]	**GGA**		309	162	192
	[40]	**LDA**		304	160	193

Table 3.18: **TOECs** of zincblende AlN in units of [GPa].

AlN	Ref.	E_{xc}		C_{111}	C_{112}	C_{123}	C_{144}	C_{155}	C_{456}
Present work		**PBE**	**EYE**	-1045	-945	-40	31	-725	-18
		PBE	**STD**	-1046	-944	-39	31	-726	-18
		PBEsol	**EYE**	-1050	-980	-46	57	-720	1
		PBEsol	**STD**	-1055	-979	-46	58	-720	2
Theory	[39]	**PBE**		-1070	-1010	-78	63	-751	-11
	[26]	**HSE**		-1125	-1036	-44	51	-789	-11.6

Our values for the **SOECs** agree well with the literature values. Our **PBE** results show only minor differences with the ones of Refs. [20, 39], while slighty larger variations are found in comparison with Ref. [27]. To the best of our knowledge, there are no experimental values for cubic AlN and InN. In the case of the **TOECs**, our values are slightly smaller than the **PBE** ones of Ref. [39]. Larger deviations are observed in the comparison to the **HSE** results of Ref. [26]. We did not find any experimental values for the **TOECs** of cubic AlN. Finally, for both **SOECs** and **TOECs** there is barely no difference between **STD** and **EYE** results.

3.3.5 Elastic constants of wurtzite AlN

For the wurtzite system there were no benchmarks performed. Due to time limitations, only one set of parameter values was used for the calculation of wurtzite AlN. This parameter set is shown in Table 3.2. Since we have only one calculation, we compare these results to different calculations in literature. In Tables 3.19 and 3.20 the calculated **SOECs** and **TOECs** of wurtzite AlN, respectively, are shown in comparison with the theoretical and experimental values available in the literature.

Table 3.19: **SOECs** of wurtzite AlN in units of [GPa].

AlN	Ref.	E_{xc}		C_{11}	C_{12}	C_{13}	C_{33}	C_{44}
Present work		**PBEsol**	**EYE**	377.0	135.1	105.7	352.9	110.9
		PBEsol	**STD**	377.0	135.2	105.7	352.8	110.9
Theory	[22]	**PBE**		413	129	96	386	126
	[37]	**LDA**		396	144	111	367	115
	[38]	**LDA**		397	143	112	372	116
	[38]	**GGA**		356	118	97	337	106
Experiment	[41]			394	134	95	402	121
	[42]			410.5	148.5	98.9	388.5	124.6

Table 3.20: **TOECs** of wurtzite AlN in units of [GPa] calculated using **PBEsol**.

AlN	C_{111}	C_{112}	C_{113}	C_{123}	C_{133}	C_{144}	C_{155}	C_{222}	C_{333}	C_{344}
EYE	-2922	-416	-246	-440	-1040	-145	-26	-2173	-923	-655
STD	-2916	-425	-246	-436	-1041	-143	-25	-2187	-923	-656

For the **SOECs**, our **PBE** and **PBEsol** values are slightly smaller than the **LDA** [37, 38] ones and somehow different from the **PBE** results of Ref. [22]. The not further specified **GGA** values from Ref. [38] are smaller than ours. Finally, to the best of our knowledge, there are no calculated or experimental values for the **TOECs** of wurtzite AlN in the literature.

3.4 Trends in elasticity of group-III nitrides

For the comparison of the group-III nitrides, we analyze the different elastic moduli introduced in Section 2.1.4 in terms of the **SOECs**. In Table 3.21 we show the values of these elastic moduli for the zincblende materials considered in this work.

Table 3.21: Bulk modulus at equilibrium B_0, shear modulus G, Young's modulus E_Y, and Poission ratio υ for the group-III nitrides in the zincblende phase.

		B_0 [GPa]	G [GPa]	E_Y [GPa]	υ
PBE	BN	371.3	386.8	861.4	0.11
	AlN	191.4	132.6	323.2	0.22
	GaN	169.3	111.0	273.2	0.23
	InN	121.3	57.5	148.9	0.30
PBEsol	BN	385.3	395.4	883.9	0.12
	AlN	199.4	132.9	326.1	0.23
	GaN	186.0	115.3	286.6	0.24
	InN	135.9	58.9	154.4	0.31

The values of the bulk moduli are very similar to the ones we calculated in Section 3.2. We observe that BN is the hardest material and InN the softest. This is shown by the bulk modulus B_0, shear modulus G, and the Young's modulus E_Y as well as by the **SOECs** themselves. The higher are the values of **SOECs** or the generalized elastic moduli, the harder is the material. Frantsevich and Bokuta [43] state that a material with the Poisson ratio $\upsilon > 0.33$, should be ductile. Every group-III nitride has a Poisson ratio $\upsilon < 0.33$ so these materials should be brittle. Pugh's rule [44] state that a material with the ratio of $G/B_0 > 0.5$, should be brittle. The ratios G/B_0 obtained using **PBE** (**PBEsol**) for the zincblende nitrides are:

$$\mathrm{BN} \to 1.04\ (1.03) \quad \mathrm{AlN} \to 0.69\ (0.67) \quad \mathrm{GaN} \to 0.66\ (0.62) \quad \mathrm{InN} \to 0.47\ (0.43)\,.$$

It can be clearly seen that all investigated crystals, except InN, are brittle. BN is the most brittle. The ambiguous behaviour of InN for both the Pugh's and Frantsevichs-Bokutas rule makes hard to classify clearly InN as brittle or ductile.

Chapter 4

Conclusions and Outlook

In this work, we investigated the elastic properties of the group-III nitrides using **DFT** calculations implemented in the software package **exciting** and the post-processing tool **ElaStic**. Benchmark tests were performed to analyze the convergence of the values of the second (**SOECs**) and third-order (**TOECs**) elastic constants and extracting the accuracy of the calculated values.

To this scope, we have introduced the δ-parameter method. This method allows for an explicit, not based on "human-eyes", measure of the accuracy of the numerical energy derivatives performed with the help of polynomial fits, which was the only "weak point" of the **ElaStic** tool. We found that, among all computational parameters, the numerical derivatives are very sensitive to the value of the parameter **gmaxvr**, which is the maximum length of the reciprocal lattice vectors for expanding the interstitial density and potential.

The obtained results for the **SOECs** and **TOECs** are also compared with experimental and theoretical values available in literature. The overall agreement for the **SOECs** is very good. The **TOECs** obtained in this work show larger deviations than the **SOECs** in comparison with experimental and other theoretical values. For BN, the **TOECs** had been calculated the first time, to the best of our knowledge. A full study of the convergence behaviour of the elastic constants of wurtzite AlN was not possible, due to time issues. We can assume that the our results for the elastic constants of wurtzite AlN are still not converged. In the analysis of common trends in the elastic behaviour of these nitrides, our work shows that BN is the hardest and InN the softest material.

In the future, the δ-parameter method could be directly integrated in the **ElaStic** tool to overcome the "human-eyes"-intervention problem. This will allow for the use of workflows for full-automatized calculations of elastic constants to the desired accuracy.

Bibliography

[1] Britannica, The Editors of Encyclopaedia. "boron nitride", 2013. URL https://www.britannica.com/science/boron-nitride. Accessed 28 February 2024.

[2] V. Zakorzhevsky. Aluminum Nitride. Concise Encyclopedia of Self-Propagating High-Temperature Synthesis, pages 16–18, 2017. doi: https://doi.org/10.1016/B978-0-12-804173-4.00007-7.

[3] W. H. Lam, W. S. Lam, and P. Lee. The Studies on Gallium Nitride-Based Materials: A Bibliometric Analysis. Materials, 401(16), 2023. doi: https://doi.org/10.3390/ma16010401.

[4] A. Bhuiyan, A. Hashimoto, and A. Yamamoto. Indium nitride (InN): A review on growth, characterization, and properties. Journal of Applied Physics, (94): 2779–2808, 2003. doi: https://doi.org/10.1063/1.1595135.

[5] A. Gulans, S. Kontur, C. Meisenbichler, D. Nabok, P. Pavone, S. Rigamonti, S. Sagmeister, U. Werner, and C. Draxl. exciting: a fullpotential all-electron package implementing density-functional the- ory and many-body perturbation theory. Journal of Physics: Condensed Matter, 26(36), 2014. doi: http://stacks.iop.org/0953-8984/26/i=36/a=363202.

[6] R. Golesorkhtabar, P. Pavone, J. Spitaler, P. Puschnig, and C. Draxl. ElaStic: A tool for calculating second-order elastic constants from first principles. Computer Physics Communications, 184(8):1861–1873, 2013. doi: http://stacks.iop.org/0953-8984/26/i=36/a=363202.

[7] F. Giustino. Materials Modelling using Density Functional Theory. Oxford University Press, 2014.

[8] G. Grimvall and E. Wohlfarth. Thermophysical properties of materials. Elsevier Science Publischer, 1986.

[9] S. Timoshenko and J. N. Goodier. Theory of Elasticity. McGRAW-HILL BOOK COMPANY, 1951.

[10] K. Brugger. Thermodynamic Definition of Higher Order Elastic Coefficients. Phys. Rev., 133:A1611–A1612, 1964. doi: http://dx.doi.org/10.1103/PhysRev.133.A1611.

[11] M. Born and R. Oppenheimer. Zur Quantentheorie der Molekeln. Annalen der Physik, 389(20):457–484, 1927. doi: http://dx.doi.org/10.1002/andp.19273892002.

[12] P. Hohenberg and W. Kohn. Inhomogeneous Electron Gas. Phys. Rev., 136: B864–B871, 1964. doi: http://dx.doi.org/10.1103/PhysRev.136.B864.

[13] W. Kohn and L. J. Sham. Self-Consistent Equations Including Exchange and Correlation Effects. Phys. Rev., 140:A1133–A1138, 1965. doi: http://dx.doi.org/10.1103/PhysRev.140.A1133.

[14] T. T. Nguyen-Dang, R. F. W. Bader, and H. Essén. Some properties of the Lagrange multiplier μ in density functional theory. International Journal of Quantum Chemistry, 22(5):1049–1058, 1982. doi: http://dx.doi.org/doi:10.1002/qua.560220517.

[15] J. P. Perdew and K. Schmidt. Jacob's ladder of density functional approximations for the exchange-correlation energy. AIP Conference Proceedings, 577(1): 1–20, 2001. doi: http://dx.doi.org/10.1063/1.1390175.

[16] J. P. Perdew, K. Burke, and M. Ernzerhof. Generalized gradient approximation made simple. Phys. Rev. Lett., 77:3865, 1996. doi: https://doi.org/10.1103/PhysRevLett.77.3865.

[17] J. P. Perdew, A. Ruzsinszky, G. I. Csonka, O. A. Vydrov, G. E. Scuseria, L. A. Constantin, X. Zhou, and K. Burke. Restoring the Density-Gradient Expansion for Exchange in Solids and Surfaces. Phys. Rev. Lett., 100:136406, 2008. doi: http://dx.doi.org/10.1103/PhysRevLett.100.136406.

[18] S. Lubeck. Private communication.

[19] Input reference for exciting fluorine. `http://exciting.wikidot.com/ref:input`. Accessed: March 7, 2024.

[20] M. de Jong, W. Chen, and T. Angsten *et al.* Charting the complete elastic properties of inorganic crystalline compounds. Sci. Data, page 150009, 2015. doi: https://doi.org/10.1038/sdata.2015.9.

[21] B. D. Fulcher, X. Y. Cui, B. Delley, and C. Stampfl. Hardness analysis of cubic metal mononitrides from first principles. Phys. Rev. B, 85:184106, 2012. doi: https://doi.org/10.1103/PhysRevB.85.184106.

[22] M. Luga, G. Steinle-Neumann, and J. Meinhardt. Ab-initio simulation of elastic constants for some ceramic materials. Eur. Phys. J. B, 58:127–133, 2007. doi: https://doi.org/10.1140/epjb/e2007-00209-1.

[23] K. Kim, W. R. L. Lambrecht, and B. Segall. Elastic constants and related properties of tetrahedrally bonded BN, AlN, GaN, and InN. Phys. Rev. B, 53: 16310, 1996. doi: https://doi.org/10.1103/PhysRevB.53.16310.

[24] J. S. Zhang, J. D. Bass, T. Taniguchi, A. F. Goncharov, Y. Chang, and S. D. Jacobsen. Elasticity of cubic boron nitride under ambient conditions. J. Appl. Phys., 109:063521, 2011. doi: https://doi.org/10.1063/1.3561496.

[25] E. F. Steigmeier. THE DEBYE TEMPERATURES OF III-V COMPOUNDS. Appl. Phys. Lett., 3:6–8, 1963. doi: https://doi.org/10.1063/1.1723561.

[26] D. S. P. Tanner, M. A. Caro, S. Schulz, and E. P. O´Reilly. Hybrid functional study of nonlinear elasticity and internal strain in zinc-blende III-V materials. Phys. Rev. Materials, 3:013604, 2019. doi: https://doi.org/10.1103/PhysRevMaterials.3.013604.

[27] U. P. Verma and P. S. Bisht. Ab-initio study of AlN in zinc-blende and rock-salt phases. Solid State Sciences, 12:665–669, 2010. doi: https://doi.org/10.1016/j.solidstatesciences.2008.12.002.

[28] I. Petrov, E. Mojab, R. C. Powell, J. E. Greene, L. Hultman, and J.-E. Sundgren. Synthesis of metastable epitaxial zinc-blende-structure AlN by solid-state reaction. Appl. Phys. Lett., 60:2491–2493, 1992. doi: https://doi.org/10.1063/1.106943.

[29] D. J. As. Recent developments on non-polar cubic group III nitrides for optoelectronic applications. Proc. of SPIE, 7608:76080G, 2010. doi: https://doi.org/10.1117/12.846846.

[30] H. Qin, X. Luan, C. Feng, D. Yang, and G. Zhang. Mechanical, Thermodynamic and Electronic Properties of Wurtzite and Zinc-Blende GaN Crystals. Materials, 10:1419, 2017. doi: https://doi.org/10.3390/ma10121419.

[31] D. Moss, A. V. Akimov, S. V. Novikov, R. P. Campion, C. R. C. R. Staddon, N. Zainal, C. T. Foxon, and A. J. Kent. Elasto-optical properties of zinc-blende

(cubic) GaN measured by picosecond acoustics. J. Phys. D: Appl. Phys., 42: 115412, 2009. doi: https://doi.org/10.1088/0022-3727/42/11/115412.

[32] S. V. Novikov, N. Zainal, A. V. Akimov, C. R. Staddon, A. J. Kent, and C. T. Foxon. Molecular beam epitaxy as a method for the growth of freestanding zinc-blende (cubic) GaN layers and substrates. J. Vac. Sci. Technol. B, 28: C3B1–C3B6, 2010. doi: https://doi.org/10.1116/1.3276426.

[33] T. Lei, M. Fanciulli, R. J. Molnar, T. D. Moustakas, R. J. Graham, and J. Scanlon. Epitaxial growth of zinc blende and wurtzitic gallium nitride thin films on (001) silicon. Appl. Phys. Lett., 59:944–946, 1991. doi: https://doi.org/10.1063/1.106309.

[34] M. Frentrup, L. Y. Lee, S. Sahonta, M. J. Kappers, F. Massabuau, P. Gupta, R. A. Oliver, C. J. Humphreys, and D. J. Wallis. X-ray diffraction analysis of cubic zincblende III-nitrides. Phys. D: Appl. Phys., 50:433002, 2017. doi: https://doi.org/10.1088/1361-6463/aa865e.

[35] S. Strite, D. Chandrasekhar, D. J. Smith, J. Sariel, H. Chen, N. Teraguchi, and H. Morkoc. Structural properties of InN films grown on GaAs substrates: observation of the zincblende polytpe. Journal of Crystal Growth, 127:204–208, 1993. doi: https://doi.org/10.1016/0022-0248(93)90605-V.

[36] J. Schörmann, D. J. As, K. Lischka, P. Schley, R. Goldhahn, S. F. Li, W. Löffler, and M. Hetterich. Molecular beam epitaxy of phase pure cubic InN. Appl. Phys. Lett., 89:261903, 2006. doi: https://doi.org/10.1063/1.2422913.

[37] V. N. Brudnyi, A. V. Kosobutsky, and N. G. Kolin. Effect of pressure and mechanical stress on the electronic properties of AlN and GaN. Phys. Solid State, 53:679–688, 2011. doi: https://doi.org/10.1134/S1063783411040093.

[38] S. P. Lepkowski, J. A. Majewski, and G. Jurczak. Nonlinear elasticity in III-N compounds: Ab initio calculations. Phys. Rev. B, 72:245201, 2005. doi: https://doi.org/10.1103/PhysRevB.72.245201.

[39] M. Łopuszyński and J. A. Majewski. Ab initio calculations of third-order elastic constants and related properties for selected semiconductors. Phys. Rev. B, 76: 045202, 2007. doi: https://doi.org/10.1103/PhysRevB.76.045202.

[40] A. F. Wright. Elastic properties of zinc-blende and wurtzite AlN, GaN, and InN. J. of Appl. Phys., 82:2833–2839, 1997. doi: https://doi.org/10.1063/1.366114.

[41] M. Kazan, E. Moussaed, and R. Naderand P. Masri. Elastic constants of aluminum nitride. Phys. Status Solidi, 4:204–207, 2007. doi: https://doi.org/10.1002/pssc.200673503.

[42] L. E. McNeil, M H. Grimsditch, and R. H. French. Vibrational Spectroscopy of Aluminum Nitride. Journal of the American Ceramic Society, 76:1132–1136, 1993. doi: https://doi.org/10.1111/j.1151-2916.1993.tb03730.x.

[43] I. N. Frantsevich, F. F. Voronov, and S. A. Bokuta. Elastic Constants and Elastic Moduli of Metals and Insulators Handbook. Naukova Dumka, Kiev, 1983.

[44] S. Pugh. XCII. Relations between the elastic moduli and the plastic properties of polycrystalline pure metals. The London, Edinburgh, and Dublin Philosophical Magazine and Journal of Science, 45(367):823–843, 1954. doi: http://dx.doi.org/10.1080/14786440808520496.

[45] M. Grimsditch, E. S. Zouboulisn, and A. Polian. Elastic constants of boron nitride. J. Appl. Phys., 76:832–834, 1994. doi: https://doi.org/10.1063/1.357757.

[46] R. J. J. Rioboo, R. Cusco, C. Prieto, C. Kopittke, S. V. Novikov, and L. Artus. Surface acoustic wave velocity and elastic constants of cubic GaN. Appl. Phys. Express, 9:061001, 2016. doi: http://doi.org/10.7567/APEX.9.061001.

Appendix A

Convergence Tables for the δ-Parameter

In this appendix, we present in Table A.1 to Table A.16 the convergence behaviour of the values of the δ-parameter with respect to the sets of computational parameters used in the calculations. Results are presented for all the materials considered in this thesis and for all distortion types.

Table A.1: Calculated values of the parameter δ as defined in Section 3.3.2 for different sets of computational parameters. Results are presented for all distortion types used in the calculation of the `SOECs` of zincblende BN calculated using `PBE`. All values are given in units of [GPa].

r	k	g	l	Dst01	Dst02	Dst03
8	8	18	8	0.13	0.10	3.24
8	8	25	12	0.61	0.23	2.63
8	12	25	12	0.13	0.20	1.80
9	8	25	12	0.21	0.03	2.10
9	12	18	8	0.56	0.26	3.66
9	12	25	12	0.01	0.03	1.87

Table A.2: Same as Table A.1 for the `SOECs` of BN using `PBEsol`. Units are [GPa].

r	k	g	l	Dst01	Dst02	Dst03
8	8	25	12	0.75	0.23	0.61
8	12	25	12	0.54	0.10	0.54
9	8	25	12	0.06	0.03	0.56
9	12	18	8	0.46	0.15	1.16
9	12	25	12	0.08	0.03	0.65

Table A.3: Same as Table A.1 for the `SOECs` of AlN using `PBE`. Units are [GPa].

r	k	g	l	Dst01	Dst02	Dst03
8	8	25	12	0.83	0.19	0.75
8	12	25	12	1.03	0.19	0.58
9	8	25	12	0.38	0.14	0.10
9	12	16	8	0.51	0.59	0.42
9	12	20	8	0.07	0.04	0.16
9	12	25	12	0.15	0.03	0.11

Table A.4: Same as Table A.1 for the `SOECs` of AlN using `PBEsol`. Units are [GPa].

r	k	g	l	Dst01	Dst02	Dst03
8	8	12	8	3.07	1.83	1.51
8	8	25	12	2.05	1.25	1.07
8	12	12	8	2.24	1.62	0.58
8	12	25	12	0.59	0.19	0.16
9	8	25	12	0.38	0.31	0.04
9	12	16	8	0.37	0.53	0.14
9	12	25	12	0.07	0.03	0.19

Table A.5: Same as Table A.1 for the `SOECs` of GaN using `PBE`. Units are [GPa].

r	k	g	l	Dst01	Dst02	Dst03
8	8	18	8	1.56	0.10	0.27
8	8	25	12	1.51	0.08	0.30
8	12	25	12	0.41	0.36	0.53
9	8	25	12	0.09	0.06	0.23
9	12	18	8	0.04	0.02	0.28
9	12	25	12	0.12	0.01	0.11
10	12	25	12	0.08	0.05	0.05

Table A.6: Same as Table A.1 for the `SOECs` of GaN using `PBEsol`. Units are [GPa].

r	k	g	l	Dst01	Dst02	Dst03
8	8	25	12	1.48	0.28	0.16
8	12	25	12	0.90	0.13	0.34
9	8	16	8	0.07	0.06	0.16
9	8	25	12	0.02	0.03	0.23
9	12	16	8	0.10	0.05	0.17
9	12	25	12	0.07	0.01	0.11

Table A.7: Same as Table A.1 for the `SOECs` of InN using `PBE`. Units are [GPa].

r	k	g	l	Dst01	Dst02	Dst03
8	8	25	12	0.32	0.62	3.99
8	12	25	12	0.24	0.28	0.83
9	8	25	12	0.73	1.20	3.87
9	12	25	12	0.11	0.36	0.86

Table A.8: Same as Table A.1 for the `SOECs` of InN using `PBEsol`. Units are [GPa].

r	k	g	l	Dst01	Dst02	Dst03
8	8	25	12	0.27	1.78	3.83
8	12	25	12	0.23	0.50	1.05
9	8	25	12	0.37	1.31	4.29
9	12	25	12	0.18	0.39	1.01

Table A.9: Same as Table A.1 for the `TOECs` of BN using `PBE`. Units are [GPa].

r	k	g	l	Dst01	Dst02	Dst03	Dst04	Dst05	Dst06
8	8	18	8	152	196	226	14	61	26
8	8	25	12	92	145	321	7	7	6
8	12	25	12	44	39	112	17	11	7
9	12	18	8	189	101	362	52	119	67
9	12	25	12	16	9	92	3	6	9

Table A.10: Same as Table A.1 for the `TOECs` of BN using `PBEsol`. Units are [GPa].

r	k	g	l	Dst01	Dst02	Dst03	Dst04	Dst05	Dst06
8	8	25	12	134	114	100	32	77	18
8	12	25	12	48	21	128	45	33	15
9	8	25	12	13	15	12	13	3	5
9	12	18	8	123	33	148	34	15	35
9	12	25	12	21	2	32	4	6	3

Table A.11: Same as Table A.1 for the `TOECs` of AlN using `PBE`. Units are [GPa].

r	k	g	l	Dst01	Dst02	Dst03	Dst04	Dst05	Dst06
8	8	25	12	206	54	36	80	59	34
8	12	25	12	71	28	14	46	29	16
9	12	16	8	45	65	64	18	80	62
9	12	20	8	7	7	11	3	21	6
9	12	25	12	12	4	14	4	19	8

Table A.12: Same as Table A.1 for the `TOECs` of AlN using `PBEsol`. Units are [GPa].

r	k	g	l	Dst01	Dst02	Dst03	Dst04	Dst05	Dst06
8	8	12	8	524	753	352	169	496	331
8	8	25	12	62	108	29	46	46	40
8	12	12	8	618	607	305	229	438	329
8	12	25	12	36	38	44	38	11	20
8	16	12	8	678	597	304	189	404	311
9	8	25	12	11	38	22	3	15	9
9	12	16	8	50	16	43	10	5	16
9	12	25	12	6	11	11	3	1	1

Table A.13: Same as Table A.1 for the `TOECs` of GaN using `PBE`. Units are [GPa].

r	k	g	l	Dst01	Dst02	Dst03	Dst04	Dst05	Dst06
8	8	18	8	194	87	27	58	117	76
8	8	25	12	195	87	29	62	115	74
8	12	25	12	161	37	19	26	88	12
9	8	25	12	13	19	41	3	11	5
9	12	18	8	4	7	55	5	7	16
9	12	25	12	19	8	27	11	11	8
10	12	25	12	1	4	15	0	1	2[†]

[†] Only for this calculation we chose $\eta_{\max}^{(\text{left})}$ = "0.04" and $\eta_{\max}^{(\text{right})}$ = "0.05".

Table A.14: Same as Table A.1 for the `TOECs` of GaN using `PBEsol`. Units are [GPa].

r	k	g	l	Dst01	Dst02	Dst03	Dst04	Dst05	Dst06
8	8	25	12	400	157	48	94	170	90
8	12	25	12	92	108	72	81	35	12
9	8	16	8	44	16	52	10	24	9
9	8	25	12	45	20	40	2	24	9
9	12	16	8	4	8	35	7	14	15
9	12	25	12	3	3	38	1	11	13

Table A.15: Same as Table A.1 for the `TOECs` of InN using `PBE`. Units are [GPa].

r	k	g	l	Dst01	Dst02	Dst03	Dst04	Dst05	Dst06
8	8	25	12	286	109	71	67	70	18
8	12	25	12	92	12	22	8	5	10
9	8	25	12	79	19	40	14	3	9
9	12	25	12	9	12	15	5	15	6

Table A.16: Same as Table A.1 for the `TOECs` of InN using `PBEsol`. Units are [GPa].

r	k	g	l	Dst01	Dst02	Dst03	Dst04	Dst05	Dst06
8	8	25	12	71	95	76	38	21	7
8	12	25	12	22	14	31	14	31	9
9	8	25	12	68	13	70	19	10	4
9	12	25	12	29	10	36	12	21	9

Appendix B

Convergence Tables for the elastic constants

In this appendix, we present in Table B.1 to Table B.16 the calculated values of the elastic constants of the materials considered in this thesis for different sets of computational parameters. All the results have been obtained using the **EYE** procedure described in Section 3.3.2.

Table B.1: Calculated values of the **SOECs** of zincblende BN in units of [GPa] for different sets of computational parameters. Only results obtained using the **EYE** method and the **PBE** exchange-correlation energy functional are included.

r	k	g	l	C_{11}	C_{12}	C_{44}
8	8	18	8	778.8	167.6	441.2
8	8	25	12	778.5	167.8	441.2
8	12	25	12	778.4	167.8	441.2
9	8	25	12	778.4	167.8	441.2
9	12	18	8	778.6	167.6	441.2
9	12	25	12	778.4	167.8	441.2

Table B.2: Same as Table B.1 for the `SOECs` of BN using `PBEsol`. Units are [GPa].

`r`	`k`	`g`	`l`	C_{11}	C_{12}	C_{44}
8	8	25	12	792.5	181.6	455.3
8	12	25	12	792.5	181.8	455.3
9	8	25	12	792.5	181.7	455.4
9	12	18	8	792.4	181.8	455.4
9	12	25	12	792.5	181.7	455.5

Table B.3: Same as Table B.1 for the `SOECs` of AlN using `PBE`. Units are [GPa].

`r`	`k`	`g`	`l`	C_{11}	C_{12}	C_{44}
8	8	25	12	280.3	146.9	176.9
8	12	25	12	279.9	147.1	176.9
9	8	25	12	279.8	147.2	176.9
9	12	16	8	280.0	147.2	176.9
9	12	20	8	279.8	147.2	176.9
9	12	25	12	279.7	147.2	176.9

Table B.4: Same as Table B.1 for the `SOECs` of AlN using `PBEsol`. Units are [GPa].

`r`	`k`	`g`	`l`	C_{11}	C_{12}	C_{44}
8	8	12	8	284.8	156.9	178.6
8	8	25	12	285.2	156.5	178.6
8	12	12	8	285.6	156.1	178.5
8	12	25	12	285.3	156.4	178.5
9	8	25	12	285.3	156.4	178.5
9	12	16	8	285.5	156.3	178.5
9	12	25	12	285.3	156.4	178.4

Table B.5: Same as Table B.1 for the `SOECs` of GaN using `PBE`. Units are [GPa].

`r`	`k`	`g`	`l`	C_{11}	C_{12}	C_{44}
8	8	18	8	250.9	128.6	144.2
8	8	25	12	250.8	128.6	144.2
8	12	25	12	250.8	128.5	144.2
9	8	25	12	250.9	128.7	144.3
9	12	18	8	250.8	128.6	144.2
9	12	25	12	250.8	128.6	144.2
10	12	25	12	250.8	128.6	144.2

Table B.6: Same as Table B.1 for the `SOECs` of GaN using `PBEsol`. Units are [GPa].

`r`	`k`	`g`	`l`	C_{11}	C_{12}	C_{44}
8	8	25	12	268.6	144.6	151.1
8	12	25	12	268.0	144.9	150.8
9	8	16	8	268.3	144.9	151.1
9	8	25	12	268.3	144.9	151.1
9	12	16	8	268.2	144.8	151.0
9	12	25	12	268.2	144.8	151.0

Table B.7: Same as Table B.1 for the `SOECs` of InN using `PBE`. Units are [GPa].

`r`	`k`	`g`	`l`	C_{11}	C_{12}	C_{44}
8	8	25	12	157.3	102.7	76.7
8	12	25	12	158.5	102.0	76.9
9	8	25	12	158.1	102.9	76.7
9	12	25	12	158.7	102.5	77.0

Table B.8: Same as Table B.1 for the `SOECs` of InN using `PBEsol`. Units are [GPa].

`r`	`k`	`g`	`l`	C_{11}	C_{12}	C_{44}
8	8	25	12	171.6	117.5	79.1
8	12	25	12	172.7	116.9	79.6
9	8	25	12	172.2	118.0	79.4
9	12	25	12	173.1	117.3	79.6

Table B.9: Same as Table B.1 for the `TOECs` of BN using `PBE`. Units are [GPa].

r	k	g	l	C_{111}	C_{112}	C_{123}	C_{144}	C_{155}	C_{456}
8	8	18	8	-4091	-1528	478	-272	-2284	-863
8	8	25	12	-4098	-1528	479	-272	-2283	-863
8	12	25	12	-4089	-1530	481	-272	-2285	-867
9	8	25	12	-4084	-1533	480	-273	-2284	-865
9	12	18	8	-4074	-1534	478	-272	-2286	-865
9	12	25	12	-4086	-1532	480	-273	-2284	-865

Table B.10: Same as Table B.1 for the `TOECs` of BN using `PBEsol`. Units are [GPa].

r	k	g	l	C_{111}	C_{112}	C_{123}	C_{144}	C_{155}	C_{456}
8	8	25	12	-4146	-1549	483	-244	-2295	-818
8	12	25	12	-4132	-1588	487	-245	-2297	-818
9	8	25	12	-4133	-1588	486	-245	-2297	-818
9	12	18	8	-4114	-1590	485	-246	-2299	-817
9	12	25	12	-4134	-1587	485	-245	-2296	-818

Table B.11: Same as Table B.1 for the `TOECs` of AlN using `PBE`. Units are [GPa].

r	k	g	l	C_{111}	C_{112}	C_{123}	C_{144}	C_{155}	C_{456}
8	8	25	12	-1048	-940	-38	31	-723	-17
8	12	25	12	-1067	-937	-39	33	-723	-18
9	8	25	12	-1052	-944	-41	32	-725	-18
9	12	16	8	-1063	-944	-41	30	-725	-19
9	12	20	8	-1047	-944	-40	32	-725	-18
9	12	25	12	-1045	-945	-40	31	-725	-18

Table B.12: Same as Table B.1 for the `TOECs` of AlN using `PBEsol`. Units are [GPa].

r	k	g	l	C_{111}	C_{112}	C_{123}	C_{144}	C_{155}	C_{456}
8	8	12	8	-1094	-999	-51	53	-718	3
8	8	25	12	-1073	-989	-53	58	-718	1
8	12	12	8	-1143	-980	-35	58	-722	3
8	12	25	12	-1051	-980	-47	57	-721	1
9	8	25	12	-1044	-980	-46	57	-721	2
9	12	16	8	-1061	-979	-46	56	-721	1
9	12	25	12	-1050	-980	-46	57	-720	1

Table B.13: Same as Table B.1 for the `TOECs` of GaN using `PBE`. Units are [GPa].

r	k	g	l	C_{111}	C_{112}	C_{123}	C_{144}	C_{155}	C_{456}
8	8	18	8	-1178	-858	-230	-61	-578	-54
8	8	25	12	-1178	-858	-230	-58	-586	-54
8	12	25	12	-1188	-856	-227	-63	-587	-54
9	8	25	12	-1184	-857	-227	-63	-588	-54
9	12	18	8	-1188	-856	-227	-63	-588	-54
9	12	25	12	-1185	-857	-228	-64	-588	-54
10	12	25	12	-1188	-857	-228	-63	-588	-54

Table B.14: Same as Table B.1 for the `TOECs` of GaN using `PBEsol`. Units are [GPa].

r	k	g	l	C_{111}	C_{112}	C_{123}	C_{144}	C_{155}	C_{456}
8	8	25	12	-1252	-952	-262	-43	-584	-41
8	12	25	12	-1234	-931	-264	-46	-585	-40
9	8	16	8	-1241	-931	-263	-45	-585	-40
9	8	25	12	-1247	-930	-263	-45	-585	-41
9	12	16	8	-1246	-930	-264	-45	-585	-40
9	12	25	12	-1251	-929	-264	-45	-584	-40

Table B.15: Same as Table B.1 for the `TOECs` of InN using `PBE`. Units are [GPa].

`r`	`k`	`g`	`l`	C_{111}	C_{112}	C_{123}	C_{144}	C_{155}	C_{456}
8	8	25	12	-750	-653	-308	-6	-266	7
8	12	25	12	-775	-649	-305	-7	-267	8
9	8	25	12	-758	-655	-310	-6	-267	6
9	12	25	12	-777	-650	-308	-6	-267	8

Table B.16: Same as Table B.1 for the `TOECs` of InN using `PBEsol`. Units are [GPa].

`r`	`k`	`g`	`l`	C_{111}	C_{112}	C_{123}	C_{144}	C_{155}	C_{456}
8	8	25	12	-824	-720	-358	16	-252	15
8	12	25	12	-831	-720	-357	21	-252	19
9	8	25	12	-825	-725	-362	16	-250	17
9	12	25	12	-840	-719	-358	16	-251	18

Appendix C

Converged elastic constants

In this appendix, we present in Tables C.1 to C.8 the converged elastic constants of the zincblende group-III nitrides obtained from our calculations. We estimate that the **SOECs** are converged up to an absolute deviation of 0.1 GPa, while a larger uncertainty of about 1 to 20 GPa in dependence of the distortion types has to be considered for the **TOECs**. The tables also contain all other theoretical and experimental values which are available in the literature, to the best of our knowledge.

Table C.1: Converged values of the **SOECs** of zincblende BN in units of [GPa]. Our values are compared here with other theoretical and experimental results which are available in the literature.

BN	Ref.	E_{xc}		C_{11}	C_{12}	C_{44}
Present work		**PBE**	**EYE**	778.4	167.8	441.2
		PBE	**STD**	778.4	167.8	440.4
		PBEsol	**EYE**	792.5	181.7	455.5
		PBEsol	**STD**	792.5	181.7	455.3
Theory	[20]	**PBE**		781	170	439
	[21]	**GGA**		800	170	450
	[22]	**GGA**		816	168	469
	[23]	**LDA**		837	182	493
Experiment	[45]			820	190	480
	[24]			798.4	172.4	469
	[25]			712	-	-

Table C.2: Same as Table C.1 for the `SOECs` of zincblende AlN in units of [GPa].

AlN	Ref.	E_{xc}		C_{11}	C_{12}	C_{44}
Present work		`PBE`	`EYE`	279.7	147.2	176.9
		`PBE`	`STD`	279.8	147.2	176.9
		`PBEsol`	`EYE`	285.3	156.4	178.4
		`PBEsol`	`STD`	285.3	156.4	178.4
Theory	[39]	`PBE`		284	167	181
	[20]	`PBE`		283	150	180
	[27]	`PBE`		315	130	245
	[26]	`HSE`		309,5	166,1	196,9
	[21]	`GGA`		309	162	192
	[40]	`LDA`		304	160	193

Table C.3: Same as Table C.1 for the `SOECs` of zincblende GaN in units of [GPa].

GaN	Ref.	E_{xc}		C_{11}	C_{12}	C_{44}
Present work		`PBE`	`EYE`	250.8	128.6	144.2
		`PBE`	`STD`	250.8	128.6	144.2
		`PBEsol`	`EYE`	268.2	144.8	151.0
		`PBEsol`	`STD`	268.2	144.8	151.0
Theory	[39]	`PBE`		255	147	148
	[20]	`PBE`		254	131	146
	[26]	`HSE`		288,4	153	166,7
	[30]	`GGA`		242.4	122.1	146.8
	[30]	`LDA`		286.9	152.8	165
	[40]	`LDA`		293	159	155
Experiment	[31]/[46]			285	149	157.7

Table C.4: Same as Table C.1 for the `SOECs` of zincblende InN in units of [GPa].

InN	Ref.	E_{xc}		C_{11}	C_{12}	C_{44}
Present work		`PBE`	`EYE`	158.7	102.5	77.0
		`PBE`	`STD`	158.7	102.5	77.0
		`PBEsol`	`EYE`	173.1	117.3	79.6
		`PBEsol`	`STD`	172.8	117.4	79.6
Theory	[39]	`PBE`		160	115	78
	[26]	`HSE`		185.2	121.7	91.5
	[40]	`LDA`		187	125	86
	[23]	`LDA`		184	116	177

Table C.5: Same as Table C.1 for the `TOECs` of zincblende BN in units of [GPa].

BN	E_{xc}		C_{111}	C_{112}	C_{123}	C_{144}	C_{155}	C_{456}
Present work	`PBE`	`EYE`	-4087	-1532	480	-273	-2284	-865
	`PBE`	`STD`	-4085	-1533	480	-273	-2285	-877
	`PBEsol`	`EYE`	-4134	-1587	485	-245	-2296	-818
	`PBEsol`	`STD`	-4135	-1587	485	-245	-2296	-819

Table C.6: Same as Table C.1 for the `TOECs` of zincblende AlN in units of [GPa].

AlN	Ref.	E_{xc}		C_{111}	C_{112}	C_{123}	C_{144}	C_{155}	C_{456}
Present work		`PBE`	`EYE`	-1045	-945	-40	31	-725	-18
		`PBE`	`STD`	-1046	-944	-39	31	-726	-18
		`PBEsol`	`EYE`	-1050	-980	-46	57	-720	1
		`PBEsol`	`STD`	-1055	-979	-46	58	-720	2
Theory	[39]	`PBE`		-1070	-1010	-78	63	-751	-11
	[26]	`HSE`		-1125	-1036	-44	51	-789	-11.6

Table C.7: Same as Table C.1 for the `TOECs` of zincblende GaN in units of [GPa].

GaN	Ref.	E_{xc}		C_{111}	C_{112}	C_{123}	C_{144}	C_{155}	C_{456}
Present work		`PBE`	`EYE`	-1185	-857	-228	-64	-588	-54
		`PBE`	`STD`	-1185	-857	-228	-64	-588	-54
		`PBEsol`	`EYE`	-1251	-929	-264	-45	-584	-40
		`PBEsol`	`STD`	-1250	-929	-265	-45	-584	-40
Theory	[39]	`PBE`		-1209	-905	-294	-45	-603	-48
	[26]	`HSE`		-1277	-976	-252	-46	-647	-49

Table C.8: Same as Table C.1 for the `TOECs` of zincblende InN in units of [GPa].

InN	Ref.	E_{xc}		C_{111}	C_{112}	C_{123}	C_{144}	C_{155}	C_{456}
Present work		`PBE`	`EYE`	-777	-650	-308	-6	-267	8
		`PBE`	`STD`	-777	-650	-308	-6	-267	8
		`PBEsol`	`EYE`	-840	-719	-358	16	-251	18
		`PBEsol`	`STD`	-832	-721	-359	14	-252	18
Theory	[39]	`PBE`		-752	-661	-357	16	-268	14
	[26]	`HSE`		-786	-701	-327	28	-290	22

Appendix D

`TOECs` tensor for cubic systems

In this appendix, we give in Table D.1 the full form of the tensor of the third-order elastic constants for materials which crystallize in the cubic zincblende structure.

Table D.1: `TOECs` tensor for cubic systems.

$c^{(3)}_{1jk}$						$c^{(3)}_{2jk}$					
C_{111}	C_{112}	C_{112}	0	0	0	C_{112}	C_{112}	C_{123}	0	0	0
C_{112}	C_{112}	C_{123}	0	0	0	C_{112}	C_{111}	C_{112}	0	0	0
C_{112}	C_{123}	C_{112}	0	0	0	C_{123}	C_{112}	C_{112}	0	0	0
0	0	0	C_{144}	0	0	0	0	0	C_{155}	0	0
0	0	0	0	C_{155}	0	0	0	0	0	C_{144}	0
0	0	0	0	0	C_{155}	0	0	0	0	0	C_{155}
$c^{(3)}_{3jk}$						$c^{(3)}_{4jk}$					
C_{112}	C_{123}	C_{112}	0	0	0	0	0	0	C_{144}	0	0
C_{123}	C_{112}	C_{112}	0	0	0	0	0	0	C_{155}	0	0
C_{112}	C_{112}	C_{111}	0	0	0	0	0	0	C_{155}	0	0
0	0	0	C_{155}	0	0	C_{144}	C_{155}	C_{155}	0	0	0
0	0	0	0	C_{155}	0	0	0	0	0	0	C_{456}
0	0	0	0	0	C_{144}	0	0	0	0	C_{456}	0
$c^{(3)}_{5jk}$						$c^{(3)}_{6jk}$					
0	0	0	0	C_{155}	0	0	0	0	0	0	C_{166}
0	0	0	0	C_{144}	0	0	0	0	0	0	C_{166}
0	0	0	0	C_{155}	0	0	0	0	0	0	C_{155}
0	0	0	0	0	C_{456}	0	0	0	0	C_{456}	0
C_{155}	C_{144}	C_{155}	0	0	0	0	0	0	C_{456}	0	0
0	0	0	C_{456}	0	0	C_{155}	C_{144}	C_{155}	0	0	0

Appendix E

TOECs tensor for wurtzite systems

In this appendix, we give in Table E.1 the full form of the tensor of the third-order elastic constants for materials which crystallize in the wurtzite structure. The explicit expression of the parameters Γ_i with $i = 1, 2, \cdots, 5$ is given below.

$$\Gamma_1 = C_{111} - C_{222} + C_{112}$$

$$\Gamma_2 = \frac{3}{4}C_{222} - \frac{1}{2}C_{111} - \frac{1}{4}C_{112}$$

$$\Gamma_3 = \frac{1}{2}C_{111} - \frac{1}{4}C_{222} - \frac{1}{4}C_{112}$$

$$\Gamma_4 = \frac{1}{2}(C_{113} - C_{123})$$

$$\Gamma_5 = \frac{1}{2}(C_{155} - C_{144})$$

Table E.1: `TOECs` tensor for wurtzite systems

$c^{(3)}_{1jk}$						$c^{(3)}_{2jk}$					
C_{111}	C_{112}	C_{113}	0	0	0	C_{112}	Γ_1	C_{123}	0	0	0
C_{112}	Γ_1	C_{123}	0	0	0	Γ_1	C_{222}	C_{113}	0	0	0
C_{113}	C_{123}	C_{133}	0	0	0	C_{123}	C_{113}	C_{133}	0	0	0
0	0	0	C_{144}	0	0	0	0	0	C_{155}	0	0
0	0	0	0	C_{155}	0	0	0	0	0	C_{144}	0
0	0	0	0	0	Γ_2	0	0	0	0	0	Γ_3
$c^{(3)}_{3jk}$						$c^{(3)}_{4jk}$					
C_{113}	C_{123}	C_{133}	0	0	0	0	0	0	C_{144}	0	0
C_{123}	C_{113}	C_{133}	0	0	0	0	0	0	C_{155}	0	0
C_{133}	C_{133}	C_{333}	0	0	0	0	0	0	C_{344}	0	0
0	0	0	C_{344}	0	0	C_{144}	C_{155}	C_{344}	0	0	0
0	0	0	0	C_{344}	0	0	0	0	0	0	Γ_5
0	0	0	0	0	Γ_4	0	0	0	0	Γ_5	0
$c^{(3)}_{5jk}$						$c^{(3)}_{6jk}$					
0	0	0	0	C_{155}	0	0	0	0	0	0	Γ_2
0	0	0	0	C_{144}	0	0	0	0	0	0	Γ_3
0	0	0	0	C_{344}	0	0	0	0	0	0	Γ_4
0	0	0	0	0	Γ_5	0	0	0	0	Γ_5	0
C_{155}	C_{144}	C_{344}	0	0	0	0	0	0	Γ_5	0	0
0	0	0	Γ_5	0	0	Γ_2	Γ_3	Γ_4	0	0	0

Acknowledgments

I thank Sven Lubeck for providing the species files used in this thesis prior to publication. I also want to thank Pasquale Pavone for guiding me through the bachelor thesis and for supporting and helping me. I want to thank my mother for supporting me the entire time and for having almost every day a warm meal cooked when I arrived home. Lastly, I want to thank Malte Meitzner for going to the gym with me so I could turn my head off for some hours and do not think about the bachelor thesis.

Selbstständigkeitserklärung

Ich erkläre ausdrücklich, dass es sich bei der vorliegende Arbeit um eine von mir selbstständig und ohne fremde Hilfe verfasste Arbeit handelt.

Ich erkläre ausdrücklich, dass ich sämtliche in der oben genannten Arbeit verwendeten fremden Quellen, auch aus dem Internet (einschließlich Tabellen, Grafiken u. Ä.) als solche kenntlich gemacht habe. Insbesondere bestätige ich, dass ich ausnahmslos sowohl bei wörtlich übernommenen Aussagen bzw. unverändert übernommenen Tabellen, Grafiken u. Ä. (Zitaten) als auch bei in eigenen Worten wiedergegebenen Aussagen bzw. von mir abgewandelten Tabellen, Grafiken u. Ä. anderer Autorinnen und Autoren (Paraphrasen) die Quelle angegeben habe.

Mir ist bewusst, dass Verstöße gegen die Grundsätze der Selbstständigkeit als Täuschung betrachtet und entsprechend der Prüfungsordnung und/oder der Allgemeinen Satzung für Studien- und Prüfungsangelegenheiten der HU (ASSP) geahndet werden.

Berlin, 18.03.2024

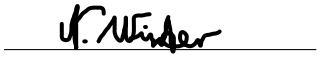

Nikita Winter